AGU PUBLICATIONS

JGR

Journal of Geophysical Research: Space Physics

RESEARCH ARTICLE
10.1002/2016JA023119

**Special Section:**
Geospace system responses to the St. Patrick's Day storms in 2013 and 2015

**Key Points:**
- Differential ionospheric response between two equinoctial storms is investigated in the 100°E meridian with conjugate hemisphere data
- Contribution of the electrodynamics and thermospheric composition change to severe negative storm effect is assessed
- Generation of equatorial irregularities is observed in the sunrise period due to disturbance electric field

**Correspondence to:**
B. R. Kalita,
bitapkalita@dibru.ac.in

**Citation:**
Kalita, B. R., et al. (2016), Conjugate hemisphere ionospheric response to the St. Patrick's Day storms of 2013 and 2015 in the 100°E longitude sector, *J. Geophys. Res. Space Physics*, *121*, doi:10.1002/2016JA023119.

Received 28 JUN 2016
Accepted 15 OCT 2016
Accepted article online 19 OCT 2016



# Conjugate hemisphere ionospheric response to the St. Patrick's Day storms of 2013 and 2015 in the 100°E longitude sector

**Bitap Raj Kalita[1], Rumajyoti Hazarika[1], Geetashree Kakoti[1], P. K. Bhuyan[1], D. Chakrabarty[2], G. K. Seemala[3], K. Wang[4], S. Sharma[5], T. Yokoyama[6], P. Supnithi[7], T. Komolmis[8], C. Y. Yatini[9], M. Le Huy[10], and P. Roy[5]**

[1]Centre for Atmospheric Studies and Department of Physics, Dibrugarh University, Dibrugarh, India, [2]Physical Research Laboratory, Ahmedabad, India, [3]Indian Institute of Geomagnetism, Navi Mumbai, India, [4]Space Weather Services, Bureau of Meteorology, Surry Hills, New South Wales, Australia, [5]Department of Physics, Kohima Science College, Kohima, India, [6]National Institute of Information and Communications Technology, Koganei, Japan, [7]Faculty of Engineering, King Mongkut's Institute of Technology Ladkrabang, Bangkok, Thailand, [8]Department of Electrical Engineering, Chiang Mai University, Chiang Mai, Thailand, [9]Space Science Center, Indonesian National Institute of Aeronautics and Space, Jakarta, Indonesia, [10]Institute of Geophysics, Vietnamese Academy of Science and Technology, Hanoi, Vietnam

**Abstract** The effects of the St. Patrick's Day geomagnetic storms of 2013 and 2015 in the equatorial and low-latitude regions of both hemispheres in the 100°E longitude sector is investigated and compared with the response in the Indian sector at 77°E. The data from a chain of ionosondes and GPS/Global Navigation Satellite Systems receivers at magnetic conjugate locations in the 100°E sector have been used. The perturbation in the equatorial zonal electric field due to the prompt penetration of the magnetospheric convective under shielded electric field and the over shielding electric field gives rise to rapid fluctuations in the $F_2$ layer parameters. The direction of IMF $B_z$ and disturbance electric field perturbations in the sunset/sunrise period is found to play a crucial role in deciding the extent of prereversal enhancement which in turn affect the irregularity formation (equatorial spread *F*) in the equatorial region. The northward (southward) IMF $B_z$ in the sunset period inhibited (supported) the irregularity formation in 2015 (2013) in the 100°E sector. Large height increase ($h_mF_2$) during sunrise produced short-duration irregularities during both the storms. The westward disturbance electric field on 18 March inhibited the equatorial ionization anomaly causing negative (positive) storm effect in low latitude (equatorial) region. The negative effect was amplified in low midlatitude by disturbed thermospheric composition which produced severe density/total electron content depletion. The longitudinal and hemispheric asymmetry of storm response is observed and attributed to electrodynamic and thermospheric differences.

## 1. Introduction

The response of the ionosphere to geomagnetic storms has received extensive attention from the scientific community due its influence over space weather. The general processes of the storm time ionospheric response is well understood, but a complete understanding that would accurately predict or nowcast the response of the ionosphere is still lacking. The ionospheric response to a storm varies widely with latitude, longitude, season, and local time. The complex nature of ionosphere-magnetosphere coupling, where two systems with different processes meet and interact [*Wolf*, 1975; *Kamide et al*., 1997, 1998; *Tsurutani et al*., 1997*; Tsurutani and Gonzalez*, 1997*; Somayajulu*, 1998] via the Earth's magnetic field lines, can create a plethora of effects in the Earth's ionosphere-thermosphere system during geomagnetic storms. The enhanced energy coupling between the solar wind and the magnetosphere-ionosphere system during magnetic storms cause ionospheric disturbances, or storms, which are manifested in terms of large deviations of ionospheric behavior from the regular quiet time behavior. The ionospheric density or electron content is found to be either enhanced (positive storm) or depleted (negative storm) [*Prolss et al*., 1988, *Rishbeth*, 1991; *Fuller-Rowell et al*., 1994; *Field and Rishbeth*, 1997; *Field et al*., 1998] depending on the local time of the storm commencement, season, latitude, and longitude of observation. The effects may vary from the $F_2$ layer to the topside [*Astafyeva et al*., 2015; *Liu et al*., 2016]. During magnetic storms, the high-latitude polar region is directly affected by the disturbed solar wind condition through the deposition of energetic particles via the near-vertical field lines when the frozen in solar wind magnetic field interacts with the geomagnetic field. At middle, low, and equatorial latitudes where geomagnetic field lines are inclined at a finite angle or

are horizontal effects due to storms occur via three processes—(1) The direct penetration of magnetospheric convective electric fields to the low latitudes; (2) the propagation of disturbed thermospheric winds generated by joule heating or ion drag effect, which transfer energy/momentum and circulate storm-induced compositional changes; and (3) the generation of disturbance electric fields by dynamo action of the disturbed wind system. In the first process, the magnetospheric convective electric field couples into the polar region where it can promptly penetrate into the low and equatorial latitudes within a few seconds [*Kikuchi et al*., 1996]. This prompt penetration electric field (PPEF) is oriented dawn to dusk, or eastward on the dayside and westward on the night side. The buildup of charges via region 1 field-aligned currents (FACs) at the solar terminator give rise to a dusk to dawn electric field which tends to shield/oppose the dawn to dusk field. The effectiveness of these two opposing electric fields at the equatorial region depends on the direction of the IMF $B_z$, with southward (northward) direction supporting the eastward (westward) penetration fields. During rapid southward turning of the IMF $B_z$, the magnetospheric dawn to dusk electric field can penetrate to the low latitudes before the development of any opposing shielding field and is called the undershielding effect. The rapid decay of region 1 FAC electric field due to the northward turning of IMF $B_z$ reinforces the shielding dusk to dawn field, and then the region 2 FAC electric field can overcome the dawn to dusk electric field [*Kelley et al*., 1979; *Kikuchi et al*., 2000], which is called the overshielding effect. These electric fields are superimposed on the quiet time *Sq* electric field causing perturbations mainly in the equatorial zonal electric field. Consequently, the equatorial electrojet (EEJ), the equatorial ionization anomaly (EIA), the equatorial spread *F* and scintillation, and the equatorial temperature and wind anomaly (ETWA), etc., are affected. The equatorial and low-latitude ionospheric response during the main phase of the storm in the first few hours is modulated by these convection electric fields. The daytime equatorial electrojet is enhanced by the undershielded eastward field during southward IMF $B_z$ turning and the counter electrojet is caused by the overshielding westward field during northward IMF turning [*Kikuchi et al*., 2010]. In the second process, the storm time particle precipitation in the auroral region sets up a series of energy transfer events via disturbed winds and tides, which propagate both toward the pole and the equator from the source region [*Fuller-Rowell et al*., 1994]. These thermospheric disturbances generate acoustic gravity waves (AGWs) which are manifested as traveling atmospheric disturbances (TADs) and traveling ionospheric disturbances (TIDs). The TIDs generated in conjugate hemisphere auroral zones during geomagnetic storms [*Hajkowicz*, 1991] due to auroral zone heating can produce significant disturbances in the equatorial region [*Fesen et al*., 1989]. Behind these disturbed winds, a disturbed thermospheric circulation is also set up [*Rishbeth*, 1975; *Fuller-Rowell et al*., 1994] and the equatorward surges carry neutral molecular-rich air from the polar region to the low- and middle-latitude region and can cause a negative effect due to enhanced recombination. Due to lower ion drag during the local night time, the wind and TIDs are more effective in the night sectors. The thermospheric effects last longer into the recovery and poststorm period due to the high inertia of the winds [*Blanc and Richmond*, 1980]. The energy deposited in the polar thermosphere due to Joule heating cause changes in the global thermospheric energy balance and thereby alters the ionospheric quiet time wind dynamo, which creates the *Sq* currents and electric fields at low and middle latitudes [*Blanc and Richmond*, 1980]. Therefore, a few hours after the storm commencement, an electric field due to the disturbed wind dynamo may also be active in the low- and middle-latitude regions and is the third process for the transmission of storm effect to these regions. The disturbed winds due to corotation creates an eastward current in the dayside midlatitudes, which in turn causes an accumulation of charges at the solar terminator due to conductivity difference in the dayside and the nightside. These charges build up a westward electric field in the dayside and an eastward field electric field in the nightside of low- and middle-latitude regions. This effect of producing a current system opposite to the *Sq* current system by the disturbed wind dynamo action is called the ionospheric disturbance dynamo [*Blanc and Richmond*, 1980] in contrast to the quiet time dynamo action which produces eastward and westward electric fields in the dayside and the nightside, respectively. The disturbance dynamo electric fields are produced late in the storm period, about 6–9 h after storm commencement [*Blanc and Richmond*, 1980; *Scherliess and Fejer*, 1997] and mostly during the storm recovery phase when the geomagnetic activity is low. Therefore, the low- and middle-latitude ionospheric response to a geomagnetic storm can be the result of the combined effect of all three mechanisms which operate concurrently for a major part of the storm. Deeper understandings of magnetospheric-ionospheric-thermospheric processes are required for accurate prediction of the electric fields [*Fejer and Emmert*, 2003] and for fixing the relative importance of the three processes in a storm time ionospheric response.

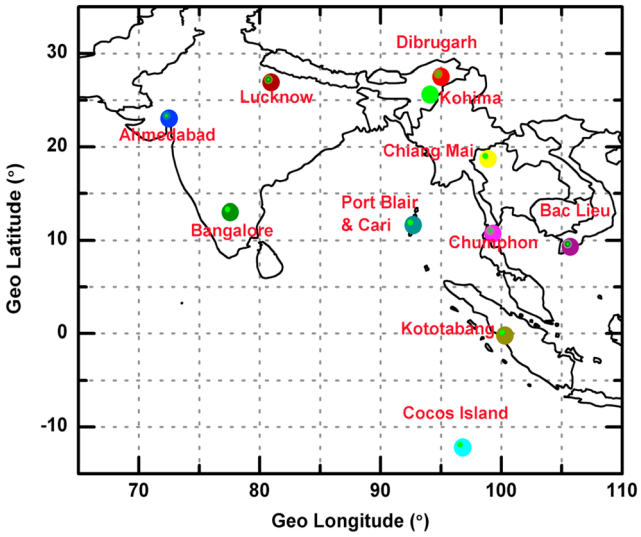


**Figure 1.** The map showing the locations of the ionospheric stations used in the study.

The strongest storm of solar cycle 24 occurred on the St. Patrick's Day (17 March) of 2015 which was marked by *Dst* index falling to less than 200 nT, *AE* crossing 2000 nT, and highest recorded *Kp* value of 8. Interestingly, on 17 March of 2013 also, a storm of lesser magnitude was observed when the minimum recorded *Dst* was 132 nT, *AE* crossed 2000 nT, and highest recorded *Kp* value was 6. The solar activity during the two storms was moderate and similar ($F_{10.7} \sim 120$ solar flux units). Both the storms were sparked by coronal mass ejection (CME) and started (6 UT) and reached the peak condition at almost same time of the day (21–23 UT). The effects of St. Patrick's Day storm of 2015 have been reported widely [*Astafyeva et al*., 2015; *Singh et al*., 2015; *Tulasi Ram et al*., 2016; *Le et al*., 2016; *Liu et al*., 2016]. *Le et al*. [2016] reported the equatorward expansion of the FAC and the auroral arc up to 60 magnetic latitude. *Liu et al*. [2016] have found asymmetry between topside and bottomside response to the storm over Millstone Hill. From TEC/topside measurements across the globe, *Astafyeva et al*. [2015] have reported the hemispheric asymmetry in ionospheric response to this storm even though the storm occurred in equinox where interhemispheric neutral flows are usually not present. The strong negative effects in the Northern Hemisphere of the Asian sector are reported and attributed mainly to compositional changes. *Singh et al*. [2015] reported the occurrence of an $F_3$ layer in the Indian sector (77°E) on 17 March daytime due to PPEF effect as well as postsunset irregularity formation with sharp height rise. *Tulasi Ram et al*. [2016] have shown that the effect of the PPEF during sunset hours is affected by the solar terminator position and that the ionospheric behavior along 100°E in the Indonesian sector was marked by the absence or inhibition of evening PRE, whereas strong PRE and associated intense scintillation was observed in the Indian longitude along 77°E in the evening period of 17 March 2015. In comparison to the 2015 storm, the effect of St. Patrick's Day storm of 2013 has not been reported widely. The equinoctial period provide an opportunity to study the differential effect of storm on latitude, longitude, and conjugate hemisphere by eliminating the seasonal effects to the first order and thereby help in fixing the storm drivers. These considerations and the observation of the quiet time longitudinal WN4 structure peak in the 100°E longitude [*Sagawa et al*., 2005; *Immel et al*., 2006; *England et al*., 2006; *Kil et al*., 2008; *Scherliess et al*., 2008; *Liu and Watanabe*, 2008, etc.] motivated us to investigate and compare the response of the ionosphere along the 100°E meridian to the St. Patrick's Day storm of 2013 and 2015 using conjugate hemisphere data. In this study, we present the latitudinal profile of the ionospheric response along the longitude of $100 \pm 5$°E using a meridional chain of stations from conjugate locations with multi-instrument data and compare the same with the response in the Indian sector at $77 \pm 5$°E. We attempt to evaluate the relative importance of the electrodynamic and thermospheric processes in the storm response.

## 2. Materials and Methods

Figure 1 shows the map of the ionospheric stations used in this study. The data from a chain of ionosondes located at Dibrugarh (27.5°N, 95°E, 43° dip), Chiang Mai (18.76°N, 98.93°E, 25° dip), Chumphon (10.72°N, 99.37°E, 5° dip), Bac Lieu (9.3°N, 105.96°E, 4° dip), Kototabang (0.2°S, 100.32°E, 19° dip), and Cocos Island (12.2°S, 96.8°E, 43° dip) and GPS/Global Navigation Satellite Systems (GNSS) TEC measurements at Dibrugarh, Kohima (25.5°N, 94.1°E, 39° dip), Cari (11.61°N, 92.71°E, 9° dip), Port Blair (11.6°N, 92.7°E, 9° dip), and Cocos Island have been used. The stations form a latitudinal chain from the northern to the southern midlatitudes along $100 \pm 5$°E. For comparison of the storm response in the Indian sector, the TEC data from Lucknow (26.91°N, 80.95°E, 41° dip), Bangalore (13.02°N, 77.67°E, 13° dip), and Ahmedabad (23.02°N, 72.5°E, 35° dip) are used. We

cover a latitudinal range of around 40° starting from the northern low midlatitude (43° dip) to the southern low midlatitude (43° dip). Chumphon and Bac Lieu are located on the geomagnetic equator (trough of EIA). The nearly magnetic conjugate pair of Chiang Mai-Kototabang is located just off the magnetic equator. Dibrugarh-Cocos Island also forms magnetic conjugate pair at low midlatitude region but are at different geographic positions relative to the respective poles. The identical equinoctial conditions during the two storms nullify the hemispherical (seasonal) effects, and conjugate hemisphere observations should provide new insights. The magnetically conjugate location of Dibrugarh and Cocos Island is unique in the sense that they are located in the transition region between low- and middle-latitude regions. The inclination of field lines in these two locations (dip ~ 43°) maximizes the effect of winds at the height of the $F_2$ layer [*Rishbeth*, 1971] and is ideally suited to study the effects of neutral winds. On the other hand due to the strongest peak of $E \times B$ drift longitudinal structure [*Kil et al*., 2008, etc.] in the 90°–100°E longitude sector, the EIA in this longitude extends poleward and the crest location is found in higher latitudes [*Sagawa et al*., 2005; *Immel et al*., 2006] as compared to other longitudes. Therefore, the density/TEC over Dibrugarh and Cocos Island are significantly affected by the EIA as well the thermospheric conditions. The ground-based magnetometer data from Tirunelveli (TIR: 8.73°N, 77.80°E, 3° dip), a station close to the dip equator, and Alibag (ABG: 18.61°N, 72.87°E, dip 26°), a station sufficiently away from the influence of the electrojet (to subtract the direct magnetospheric effects), have been used following the methodology suggested by *Chandra and Rastogi* [1974] to obtain the EEJ which serves as the indicator of the equatorial electric field.

## 3. Data

The ionosonde data in Chiang Mai, Bac Lieu, Chumphon, and Kototabang are obtained from Southeast Asia Low latitude Ionospheric Network (SEALION) which is operated by the National Institute of Information and Communication Technology, Japan (http://seg-web.nict.go.jp/sealion/). These are frequency-modulated continuous wave (CW) ionosondes. Canadian Advanced Digital Ionosonde (CADI) is operated by Dibrugarh University from July 2010. In Cocos Island, an IPS 5D ionosonde is operated by the Bureau of Meteorology, Australia from August 2008. The IPS 5D sweeps from 1 to 21.5 MHz and records ionograms every 5 min. The ionograms of these stations are manually scaled to obtain the $F_2$ layer critical frequency $f_oF_2$, the $F_2$ layer real height $h_mF_2$, and the virtual height $h'F_2$ at fixed frequencies (2.5–8 MHz). The real height of the $F_2$ layer peak density $h_mF_2$ is obtained by real height inversion of ionograms using POLAN [*Titheridge*, 1985]. The TEC and scintillation data are obtained from Novatel GPS station 6 GNSS receiver measurements at Dibrugarh and Kohima and Novatel GSV4004B receiver at Ahmedabad. The procedure to estimate the vertical TEC is explained in *Bhuyan and Hazarika* [2012]. The GNSS receivers in Dibrugarh and Kohima are calibrated by a Novatel proprietary software. The GPS receiver in Ahmedabad is calibrated with a similar receiver in Ahmedabad which is part of GAGAN (GPS Aided Geo-Augmented Navigation) network which is a Satellite Based Augmentation System (SBAS) developed by Indian Space Research Organization (ISRO) in collaboration with Airports Authority of India (AAI). The receiver bias for the GAGAN receivers is corrected using a methodology described in *Acharya et al*. [2007]. For Novatel receivers, the satellite bias values are periodically obtained from the site (http://aiuws.unibe.ch/spec/dcb.php#p1c1) and these values are used periodically to recalibrate the data. The TEC obtained from the International GPS Service (IGS) stations at Lucknow, Bangalore, Cari, Port Blair, and Cocos Island is also used and available at (ftp://cddis.gsfc.nasa.gov/pub/gps/data/daily/) in RINEX format. RINEX files are converted to TEC using the GPS-TEC program [*Seemala and Valladares*, 2011] downloaded from http://seemala.blogspot.com/. The vertical TEC (here after VTEC) from all the visible satellites with elevation mask of 50° has been considered to reduce effect of single-shell model in VTEC conversion and multipath [*Rama Rao et al*., 2006]. The residual error due to transformation into VTEC using single-shell model for elevation $> 50°$ is less than 1 TEC unit. To eliminate multipath effect for the scintillation data, the elevation angle is cutoff at 30°. The IMF $B_z$ data are taken from ACE (Advanced Composition Explorer) and Wind satellite, which time shifted to Bow Shock Nose. To describe the geomagnetic disturbance fields in midlatitudes with high time resolution (i.e., 1 min), symmetric (*SYM-H*) disturbance index data are taken from Kyoto World Data Center website (http://wdc.kugi.kyoto-u.ac.jp/wdc/Sec3.html). The solar wind velocity (SW), *AE*, and *ASY-D* data are taken from http://cdaweb.gsfc.nasa.gov/istp_public/ website. The auroral electrojet index, *AE*, is used as indicator of substorm activity, and the asymmetric ring current index *D* component, *ASY-D*, is used as indicator of field-aligned currents (FACs) following *Wei et al*. [2011]. The thermospheric neutral composition variations in terms of ($O/N_2$) described

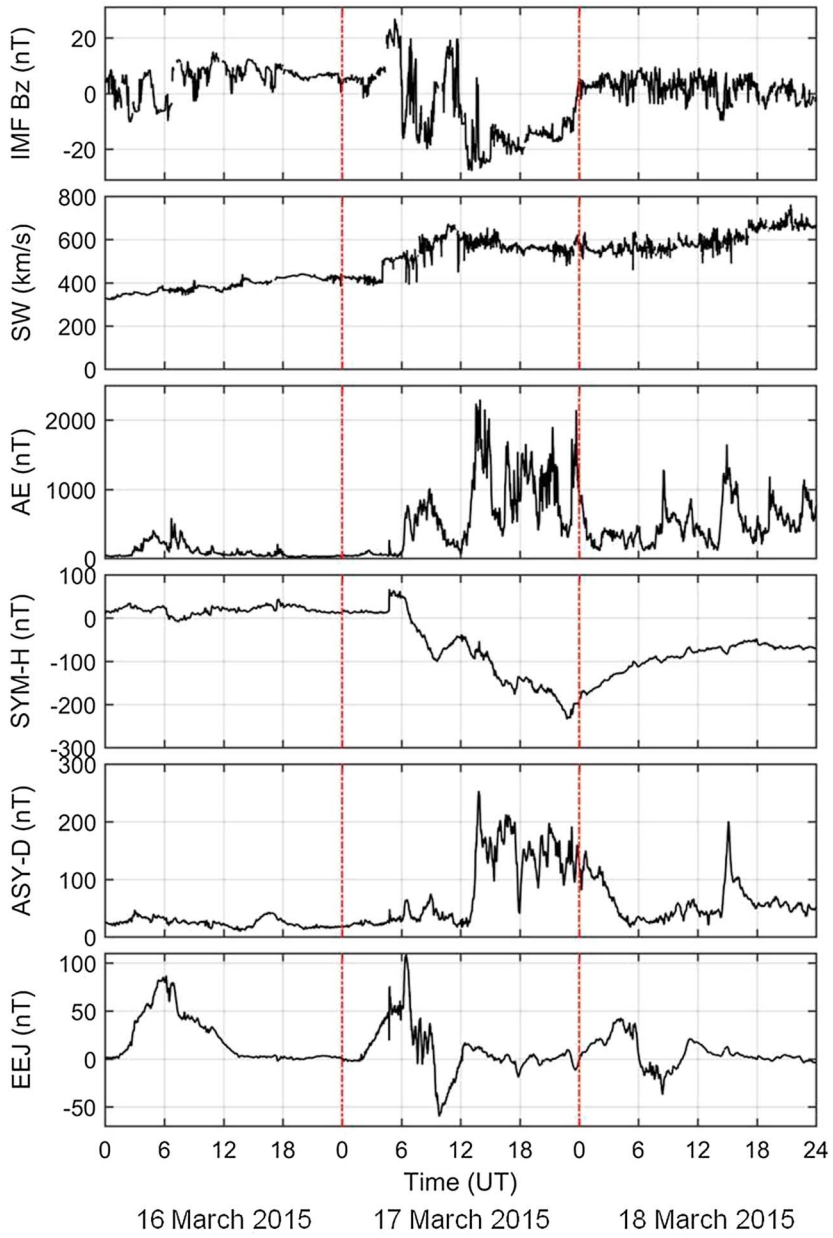


**Figure 2.** The *z* component of interplanetary magnetic field IMF $B_z$, the solar wind speed, the auroral elctrojet index *AE*, the symmetric ring current index *SYM-H*, the asymmetric ring current index *D* component *ASY-D*, and equatorial electrojet (EEJ) indices for the period of 16–18 March 2015.

in this study has been obtained from Global Ultraviolet Imager (GUVI) instrument on board Thermosphere, Ionosphere, Mesosphere, Energetics and Dynamics (TIMED) spacecraft (http://guvi.jhuapl.edu/).

## 4. Results and Discussion

The response of the ionosphere to the 17–18 March 2015 super storm is discussed first, followed by 2013 storm and the comparison. The geomagnetic activity indices during 16–18 March 2015 are shown in Figure 2. The sudden storm commencement (SSC) occurs at 4:45 UT followed by main phase at around 6 UT and recovery phase starting at around 24 UT of 17 March as seen from the *SYM-H* index. We present the response of the ionosphere to the enhanced magnetic activity on 17 March in the form of a time history

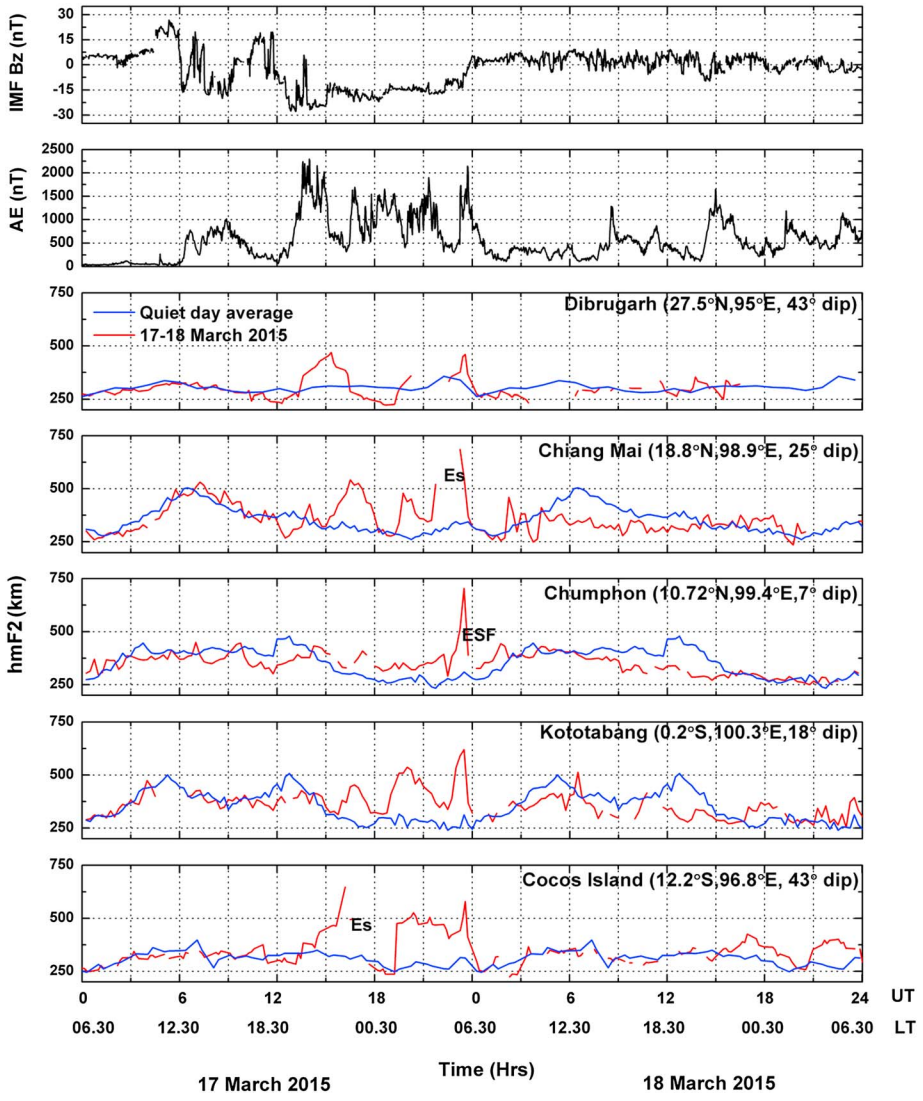


**Figure 3.** The variation of $F_2$ layer height $h_mF_2$ in the 100°E longitude on 17 and 18 March 2015. Unmarked data gaps are due to lack of data during these periods.

of the events associated with the onset of the storm. The response of all the ionospheric parameters to the triggering geomagnetic conditions is examined together and the probable mechanisms are discussed.

### 4.1. The Electrodynamic Response

The response of the $F_2$ layer parameters $h_mF_2$ and $N_mF_2$ obtained from the meridional chain of ionosondes at Dibrugarh, Chiang Mai, Chumphon, Kototabang, and Cocos Island to the variations of $z$ component of the interplanetary magnetic field (IMF) $B_z$ on 17 and 18 March are shown in Figures 3 and 4, respectively. The GPS/GNSS TEC variations over Dibrugarh, Kohima, Ahmedabad, Cari, and Cocos Island are shown in Figure 5. Five quiet days before and after 17 March 2015 are used as control days, and their average is superimposed for estimation of storm-induced changes. We observe that the $h_mF_2$ variation during daytime of 17 March is in a different scale than the variation at night and the height variation on the 18 March during the recovery phase of the storm. Therefore, to discuss the response of the height of the $F_2$ layer peak density $h_mF_2$ during daytime of 17 March, a blown up version of 0–15 UT period of Figure 3 is shown in Figure 6 and the critical events on the time (UT) axis are marked by vertical lines which provide a snapshot of the magnetospheric and ionospheric conditions at those instances. After storm commencement, fluctuations of significant amplitude can be seen in the ionospheric parameters of all the stations. The simultaneous height

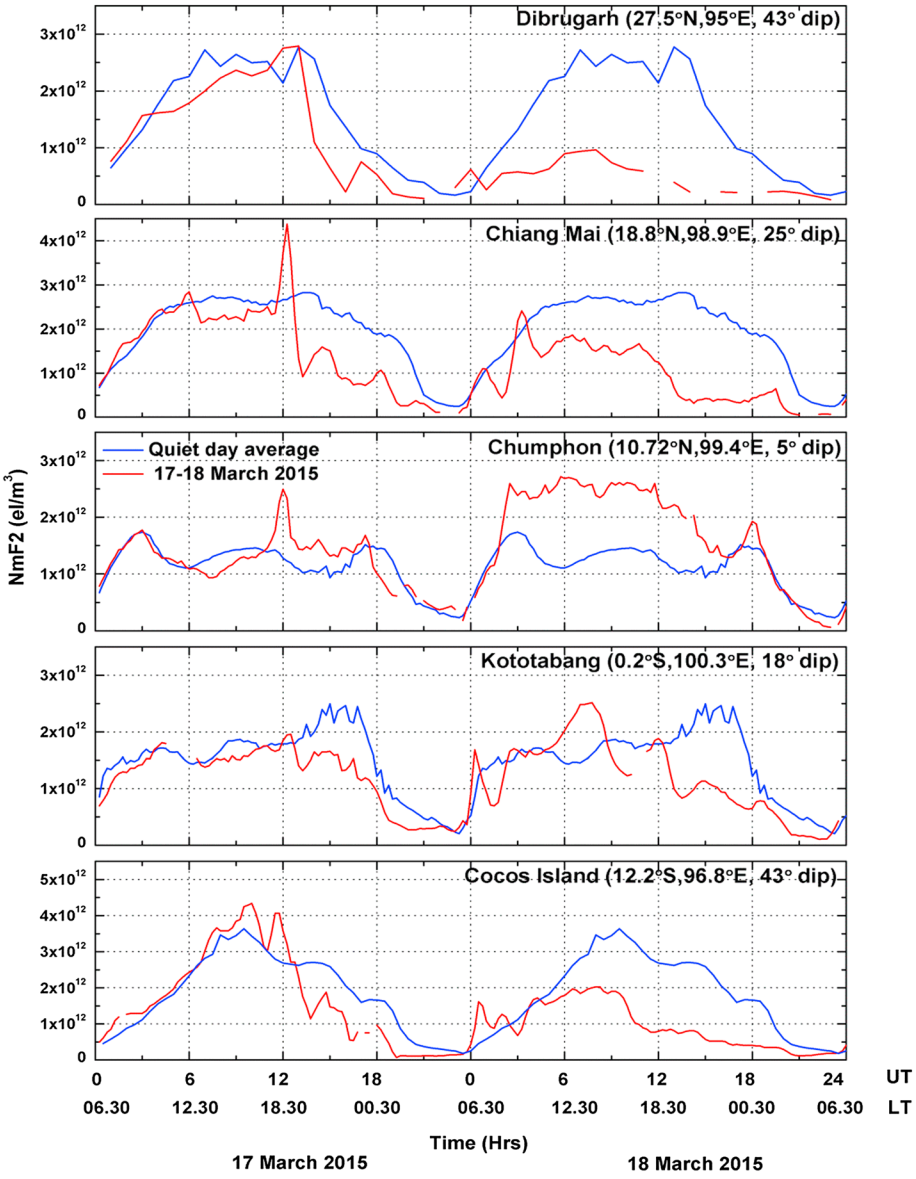


**Figure 4.** The variation of $N_mF_2$ in the 100°E longitude on 17 and 18 March 2015. Different scales are used for each station to highlight the fluctuations.

($h_mF_2$) fluctuations (Figures 3 and 6) are indicative of the penetration of the magnetospheric convective electric fields to the equatorial and low-latitude regions due to the sudden turnings of the IMF $B_z$ component. The effect of winds on the daytime height variations is minimum as interhemispheric neutral winds are not significant in equinox. The daytime fluctuations are more prominent on the $h_mF_2$ variations over Chumphon at the magnetic equator, whereas nighttime variations are higher in the low latitudes. The superposition of the short-duration PPEF on the *Sq* electric field creates perturbation on the zonal electric field and lead to fluctuations in the vertical $E \times B$ drift. The perturbed vertical drifts are manifested as sharp and rapid height variation over the equatorial region. The first southward turning of the IMF $B_z$ was observed at around 6:20 UT (vertical line 1) with increase in *AE* indices due to energy input in the polar region. The rapid and large deviations of the $h_mF_2$ over Chumphon from the quiet day values may be used to infer the presence of prompt penetration convection electric fields [*Balan et al.*, 2011; *Wei et al.*, 2011] and in this case the $h_mF_2$ increase of about 65 km in less than 30 min and a deviation of about 60 km from the quiet day value over Chumphon (at around 6:45 UT) can be observed. The in-phase superposition of the dawn to dusk prompt penetration electric field with the quiet time eastward zonal electric field leads to the enhancement of the

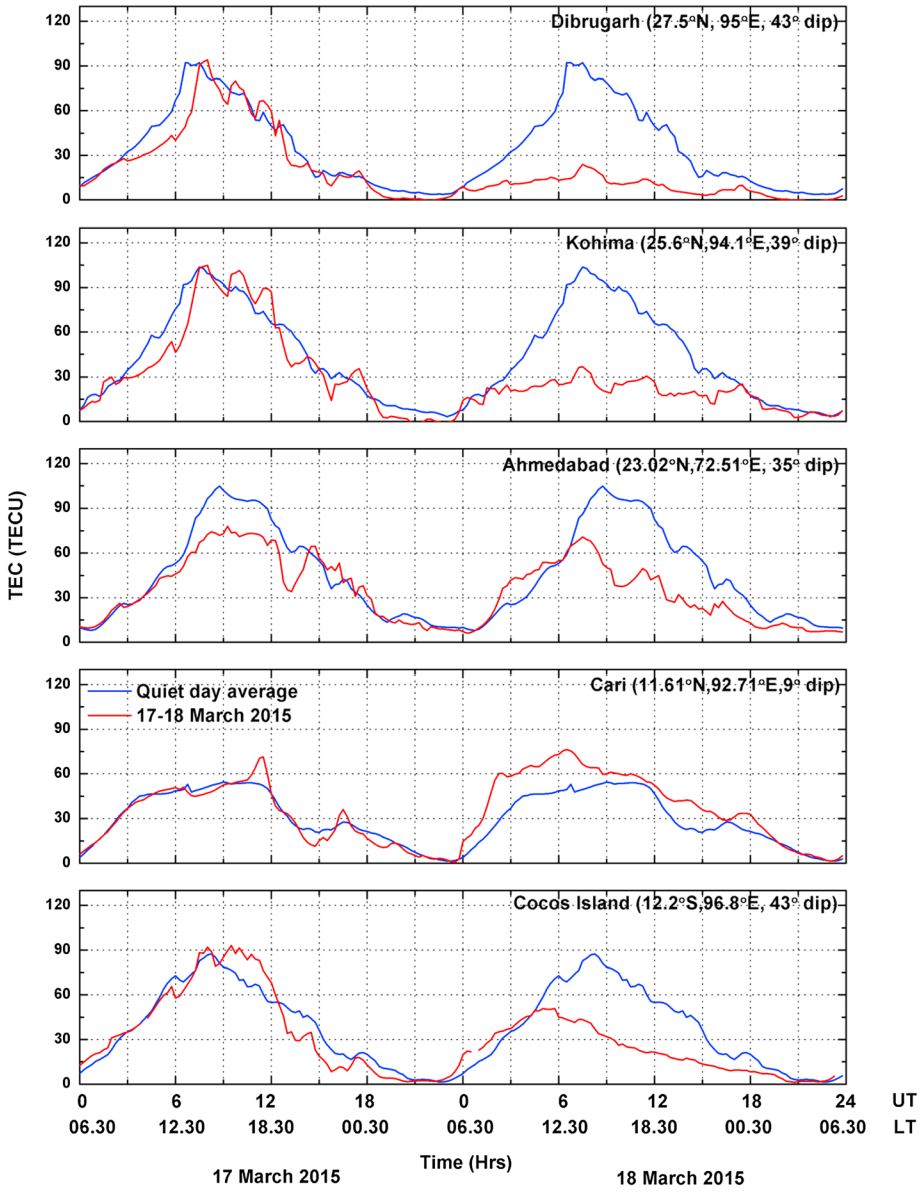


**Figure 5.** The variation of TEC in the 100°E longitude on 17 and 18 March 2015 and comparison with Ahmedabad in the 77°E longitude.

vertical $E \times B$ drift and consequently a stronger equatorial plasma fountain. Moderate $N_mF_2$ depletion over equatorial stations (Figure 4) Chumphon, Chiang Mai, and Kototabang and the TEC depletion over Cari as compared to the quiet day can be observed around 6–7 UT (Figure 5). The low-latitude density/TEC in the midday period (12–19 LT) is highly influenced by the equatorial anomaly due to the transport of the plasma from the equator by the fountain effect. Therefore, the $N_mF_2$/TEC fluctuations over Dibrugarh, Kohima, Ahmedabad, and Cocos Island in the 06–12 UT (12–19 LT) period are related to the EIA fluctuations but are delayed due to the time required for the plasma to rise to higher altitude in the equatorial region and then diffuse under gravity/pressure gradient via field lines to the low latitudes [*Sastri*, 1990; *Chakrabarty and Hajra*, 2009]. The IMF $B_z$ subsequently turned northward (vertical line 2) but made temporary southward excursion during 7:10–7:50 UT. The consequent overshielding westward electric field opposed the quiet time upward vertical drift and as a result the height of the layer was reduced over the magnetic equator (Chumphon). The $h_mF_2$ over Dibrugarh, Chiang Mai in the Northern Hemisphere, and Kototabang and Cocos Island in the Southern Hemisphere also decreased. The presence of shielding electric field in the equator during this

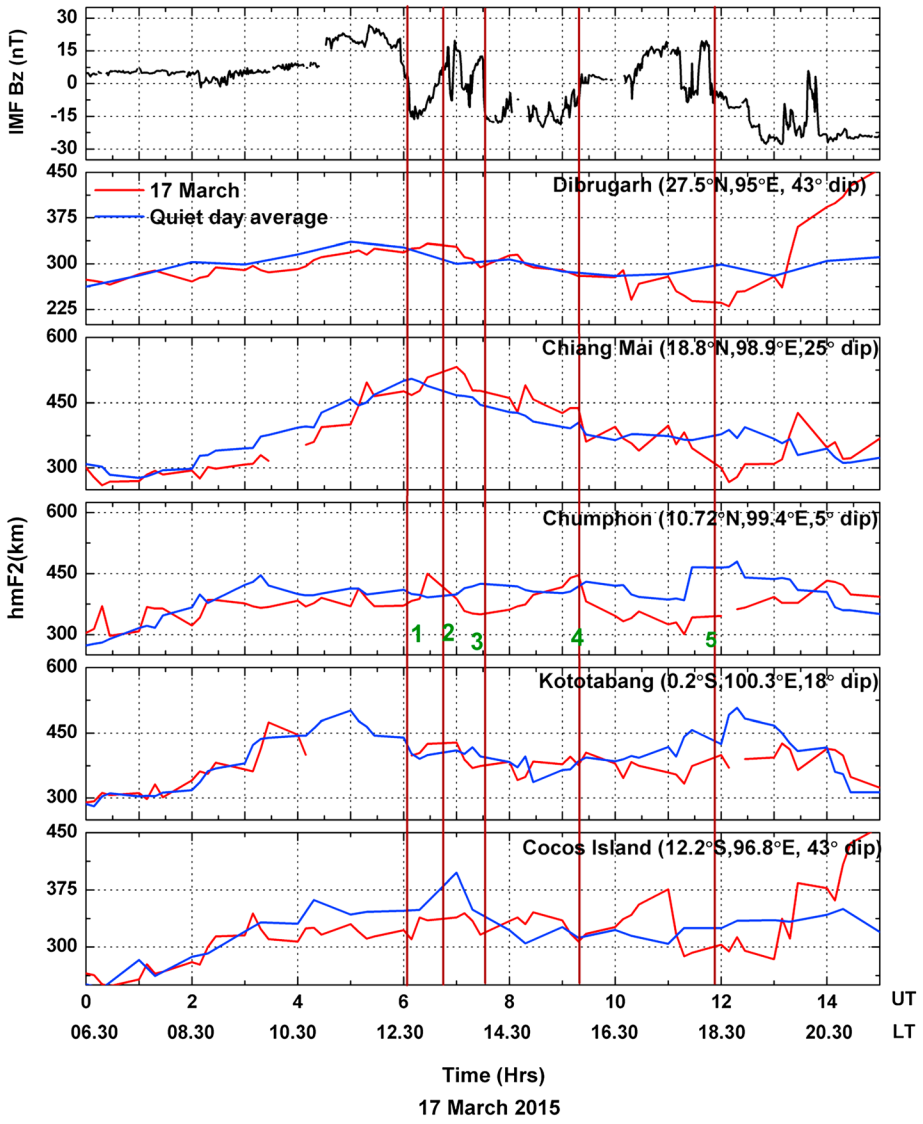


**Figure 6.** The variation of $h_mF_2$ in the 100°E meridional chain on 17 March 2015.

period is confirmed by the decreasing electrojet strength (Figure 2). Consequently, the equatorial plasma fountain is weakened, and the equatorial $N_mF_2$ is stabilized. Subsequently, the IMF $B_z$ turned southward around 7:45 UT (vertical line 3) and remained so for an extended duration. The weak electrojet and the insignificant $h_mF_2$ change over Chumphon during this period indicate that in this case the quiet time zonal electric field in the local afternoon sector (08–10 UT) was not altered significantly. The increase in *ASY-D* (Figure 2) during this period suggests increase in region 2 field-aligned currents. The low-latitude TEC in the 100°E longitude sector (Dibrugarh, Kohima, and Cocos Island) fluctuated rapidly, whereas the TEC at the crest of EIA in the 77°E longitude sector (Ahmedabad) was saturated (Figure 5). The fluctuations in the TEC could be due to fluctuating strength of the equatorial fountain. The northward turning of IMF $B_z$ after 9 UT (vertical line 4) which remained so till around 12 UT caused the $h_mF_2$ to decrease at all the stations. The presence of westward electric field in equatorial and low latitudes can be inferred from the counter electrojet event and the lower values of the $h_mF_2$ as compared to the quiet day values. The prolonged southward IMF $B_z$ previously (7:50–9:30 UT) allowed the growth of the overshielding westward electric field. The maximum $N_mF_2$ over Chumphon and Chiang Mai (and minor enhancement in Kototabang) were registered around 11:30–12 UT (vertical line 5) coinciding with the recovery from the minimum of $h_mF_2$ when the IMF $B_z$ was still pointing north. The $N_mF_2$ over Chumphon and Chiang Mai almost doubled within just 1 h and showed enhancements

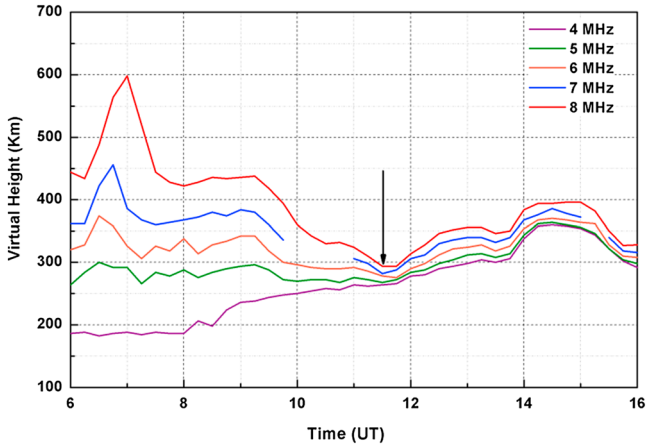


**Figure 7.** The variation of isodensity contours over Chumphon. The compression of the *F* layer around 11:30 UT is shown by an arrow.

of about 40% from the quiet time value. The asymmetry between Chiang Mai and Kototabang is noteworthy and could be related to the slightly different dip angles or the hemispherical asymmetry in the EIA. The TEC in the equatorial region (Cari) of 100°E longitude sector exhibited a peak around 12 UT, whereas the $N_mF_2$/TEC at low latitude showed smaller enhancements at slightly earlier time. The $N_mF_2$/TEC enhancements in the same period are also reported from the Indian sector at 77°E longitude [*Singh et al*., 2015]. As the IMF $B_z$ was northward with the substorm in the recovery phase from 9:45 to 11:15 UT, the $h_mF_2$ in all equatorial stations had continuously decreased during this period. In contrast, the $h_mF_2$ over low midlatitude stations Dibrugarh and Cocos Island increased during 10–11 UT hours, which were followed by smaller height increase in Chiang Mai and Kototabang after 11 UT. This pattern of height variation indicates the propagation of an equatorward meridional wind from both hemispheres. Therefore, the reduction of the equatorial upward vertical drift by the westward overshielding electric field and the reduction in downward diffusion along field lines due to the upward push by the equator ward winds combined to weaken the forward plasma fountain and created the reverse fountain effect [*Balan and Bailey*, 1995]. This resulted in accumulation of plasma in the equatorial region. The mechanism of $N_mF_2$ enhancement over Chumphon where the effect of wind on height variation is negligible due to nearly horizontal field lines may be different. It appears that the plasma under the influence of downward drift due to the westward over shielding field and the rapid recombination at the bottomside got compressed into a very dense layer. This is confirmed by the temporal variation of the isodensity contours scaled at 4–8 MHz (Figure 7) over Chumphon which show a clear merging of the contours around 11:30 UT. The local time (18 h) of this enhanced density corresponds to the sunset period, when normally the quiet time prereversal enhancement (PRE) of the zonal eastward electric field is observed and which is manifested as enhancement of vertical drift and $F_2$ layer height at the equator. On 17 March, the IMF $B_z$ was northward till about 12 UT (18:40 LT) and a counter electrojet was going on which indicated that a westward disturbance field was dominant over 100°E longitude and suppressed the PRE in the eastward zonal electric field. This is also supported by the $h_mF_2$ data which shows significantly lower heights (350 km) over Chumphon during 12 UT of 17 March as compared to the quiet day average (460 km). The southward turning of the IMF $B_z$ in the post 12 UT period did help the $h_mF_2$ to climb to 370 km, but it was still much lower than the quiet day height during this period. This can be ascribed to the reversing of the background *Sq* electric field (vertical drift) to westward polarity (downward drift) in the postsunset period. The prereversal enhancement of vertical drift is a precursor to formation of irregularity and plasma bubbles, plumes, etc. [*Fejer et al*., 1999; *Abdu*, 2001; *Kelley et al*., 2011] which are manifested as spread *F* in ionograms and scintillation in the L band/VHF over the equatorial region [*Morse et al*., 1977; *Rastogi and Woodman*, 1978; *Basu et al*., 1980; *Dasgupta et al*., 1983; *Basu et al*., 1996; *Rama Rao et al*., 2005]. On the evening (12–15 UT) of 17 March, no significant spread *F* was observed over equatorial region of 100°E, whereas *Singh et al*. [2015] reported spread *F* over Indian sector at 77°E longitude. Noteworthy difference between TEC over 100°E (Dibrugarh/Kohima/Cocos Island) and 77°E (Ahmedabad) can be observed around 15 UT of 17 March. While the TEC in 100°E was lower than the quiet day value, the TEC in Ahmedabad was similar to that on the quiet day. The sharp TEC depletions in the low latitude of 100°E longitude in the post 12 UT period (LT postsunset) shows the effect of westward electric field during 9–12 UT, which inhibited the PRE and consequently reduced the density in the EIA crest region. Figure 8 shows the S4 index measured by GNSS receivers over Dibrugarh, Kohima, and Ahmedabad on 16, 17, and 18 March. No L band scintillation was observed over Dibrugarh/Kohima around 12–15 UT on 17 March, whereas significant scintillation was observed over Ahmedabad. This suggested that irregularities were formed in the Indian longitude sector

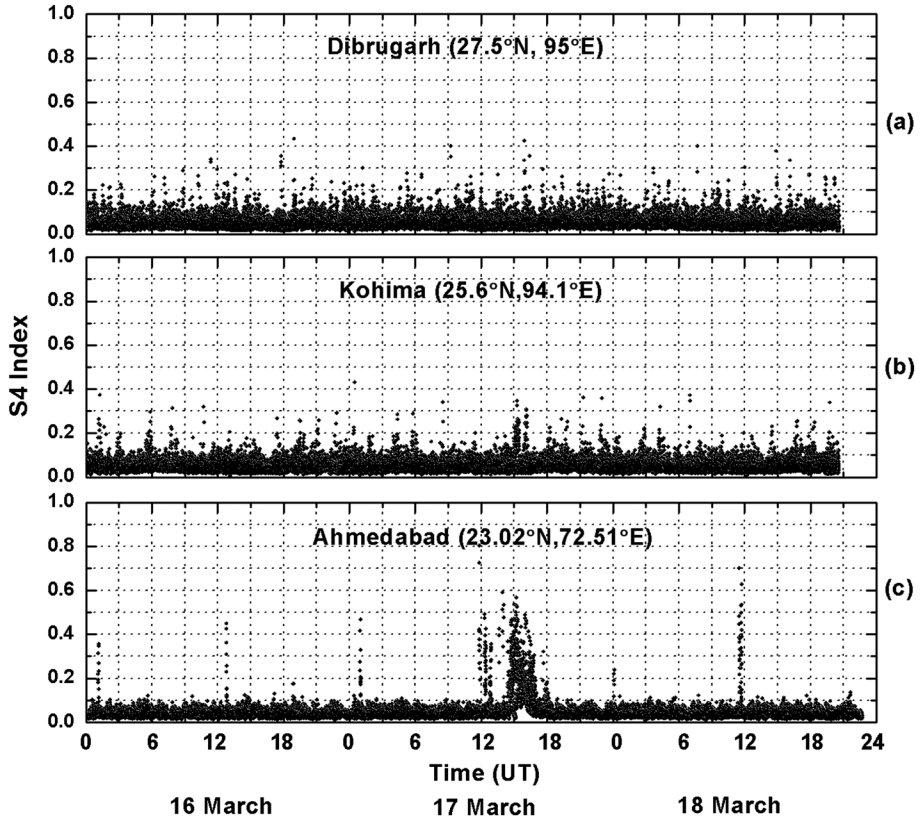


**Figure 8.** The S4 index for 16–18 March 2015 showing the scintillations over Ahmedabad in the local evening of 17 March. The elevation angle is cutoff at 30°.

on 17 March as confirmed by *Singh et al*. [2015] and *Tulasi Ram et al*. [2016]. The presence of an eastward PPEF due to the southward turning of the IMF $B_z$ after 12 UT coincided with the sunset period (PRE occurrence time) in the 77°E (LT = UT + 5:30) longitude sector and thereby supported the irregularity formation. On the other hand northward IMF $B_z$ prior to 12 UT inhibited PRE in the 100°E longitude sector which is about 1.5 h ahead in LT. The absence (presence) of PRE in the 100°E (77°E) longitude shows the critical role played by the direction of interplanetary magnetic field in storm time response of the ionosphere and the modification of the quite time equatorial electrodynamics by storm-induced currents/fields. The IMF $B_z$ remained southward from 12 UT (18:30 LT) to midnight (6:30 LT) with the minimum IMF $B_z$ values of around 30 nT being recorded during 13–14 UT. The height variations ($h_mF_2$) more or less followed the modulation of the IMF $B_z$ and the substorm development-recovery phase as indicated by variations in *AE* index. The large substorm development (Figure 2) was followed by height increase over all the stations during 13–14 UT. The quiet time electric fields during this period are mainly westward providing downward drift, and therefore, the penetration electric field perturbation can be inferred from the large height increases. The equatorward neutral winds amplified the height increase over low midlatitude stations (the different scale in Dibrugarh and Cocos Island is to be noted) as compared to the equatorial stations. The higher $N_mF_2$ (Figure 4) across all the stations was due to the reduced recombination at higher altitude. The height enhancements during 16 UT and 19 UT seem to be related to the meridional winds as the corresponding height change over Chumphon at the equator was insignificant. Sudden increase in the $h_mF_2$ (Figure 3) is observed across all the station during 23:00–23:30 UT (05:00–05:30 LT). The *F* layer over the equatorial stations Chumphon, Chiang Mai, and Kototabang recorded their highest $h_mF_2$ of around 700 km with the formation of $F_3$-like ledge at higher altitude. This large (~100%) increase from the quiet time value is due to large vertical drift caused by an eastward electric field or equator ward neutral meridional winds. The simultaneous increase (with magnetic equator) across all latitudes points favorably to an eastward electric field which may result from the PPEF associated with substorm development and recovery or/and the disturbance dynamo electric

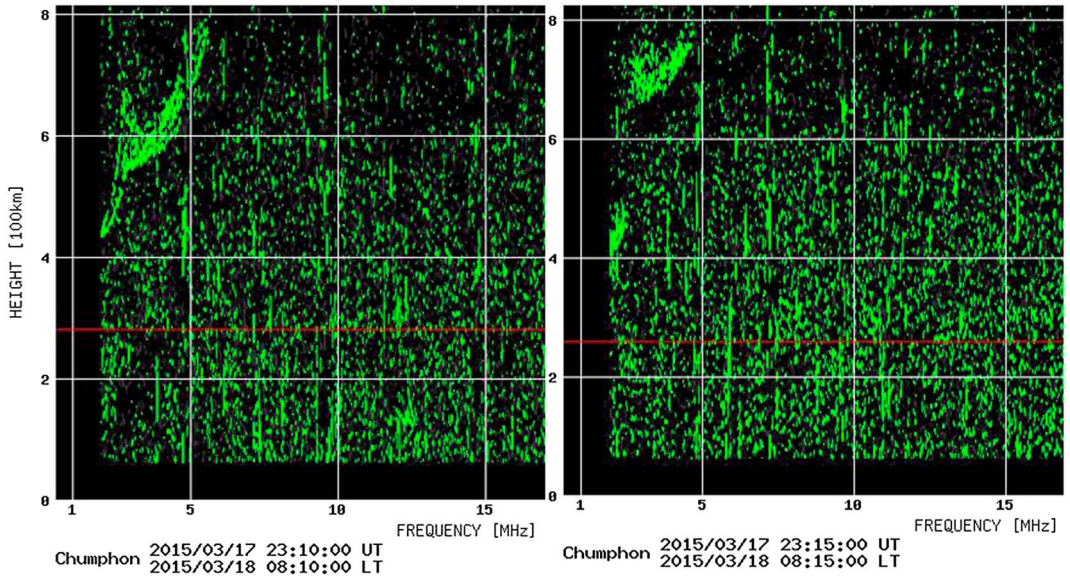


**Figure 9.** The ionograms showing the spread *F* over Chumphon in the sunrise period of 18 March 2015.

field which peak in the sunrise period [*Scherliess and Fejer*, 1997]. The large upward movement of the $F_2$ layer produced irregularities, which manifested as spread *F* over Chumphon, and the sample ionograms are shown in Figure 9. This is an interesting result considering the unusual time of development of spread *F* when the *F* layer density is very low and sharp bottomside density gradient are not present. Intense sporadic $E_s$ was observed over Chiang Mai preceding the spread *F*. The $N_mF_2$ in the low-latitude region remained lower than the quiet time values during the nighttime, whereas the TEC also decreased in the postmidnight hours (18 UT).

The IMF Bz and all other indices recovered by the morning of 18 March, but the equatorial electrojet development was subdued as compared to the quiet day, and by 6 UT counter electrojet was observed (Figure 2). The $h_mF_2$ over equatorial stations (Figure 3) were lower than the quiet day average value indicating a weaker vertical $E \times B$ drift. The $N_mF_2$/TEC over equatorial (low latitude and low midlatitude) region was higher (lower) than quiet day's value suggesting a underdeveloped EIA. Significant longitudinal, latitudinal, and hemispherical differences in ionospheric response on 18 March are observed. In the local afternoon period (6–12 UT) of 18 March, the TEC over Ahmedabad was lower by about 50%, whereas the TEC over Dibrugarh, Kohima, and Cocos Island was lower by about 75%, 70%, and 50%, respectively, as compared to the corresponding quiet time values. *Singh et al*. [2015] have also reported TEC/$N_mF_2$ depletion in the low-latitude Indian sector for the same time period, but the magnitude of the depletion is smaller than those observed in the Northern Hemisphere 100°E longitude. The TEC over equatorial station Cari was higher by about 60% as compared to quiet day average and higher than low-latitude TEC. Therefore, the EIA was completely inhibited in the 100°E longitude on 18 March 2015. The EIA in these longitude sectors develops around 06 UT and reach the maximum value between 07 and 10 UT [*Rama Rao et al*., 2006; *Bhuyan and Borah*, 2007] which can be also be confirmed from the comparison of the temporal evolution of the quiet day average TEC of Dibrugarh, Kohima, Cari, and Cocos Island (Figure 5). On 18 March, up to around 06 UT, the TEC of over Ahmedabad and Cocos Island is higher than the quiet day average. In contrast, the TEC over Dibrugarh is lower than the quiet day average from the previous night and at 6 UT, the TEC is lower than the quiet day average by about 50%. The solar diurnal variation of TEC in Dibrugarh is almost indiscernible on 18 March, and the negative effect is stronger than Kohima which is nearer to the EIA crest. Therefore, the depletions over Ahmedabad and Cocos Island appear to be the result of EIA inhibition, whereas the TEC over Dibrugarh and Kohima was affected by some other forcing mechanism in addition to the absence of the EIA during the postnoon period. The negative storm effect in midlatitudes is usually attributed to the thermospheric composition change by storm-induced equatorward winds from the polar region [*Fuller-Rowell et al*., 1994; *Liou et al*., 2005, etc.]. Dibrugarh being located in the outer edge of the EIA and in the transition region

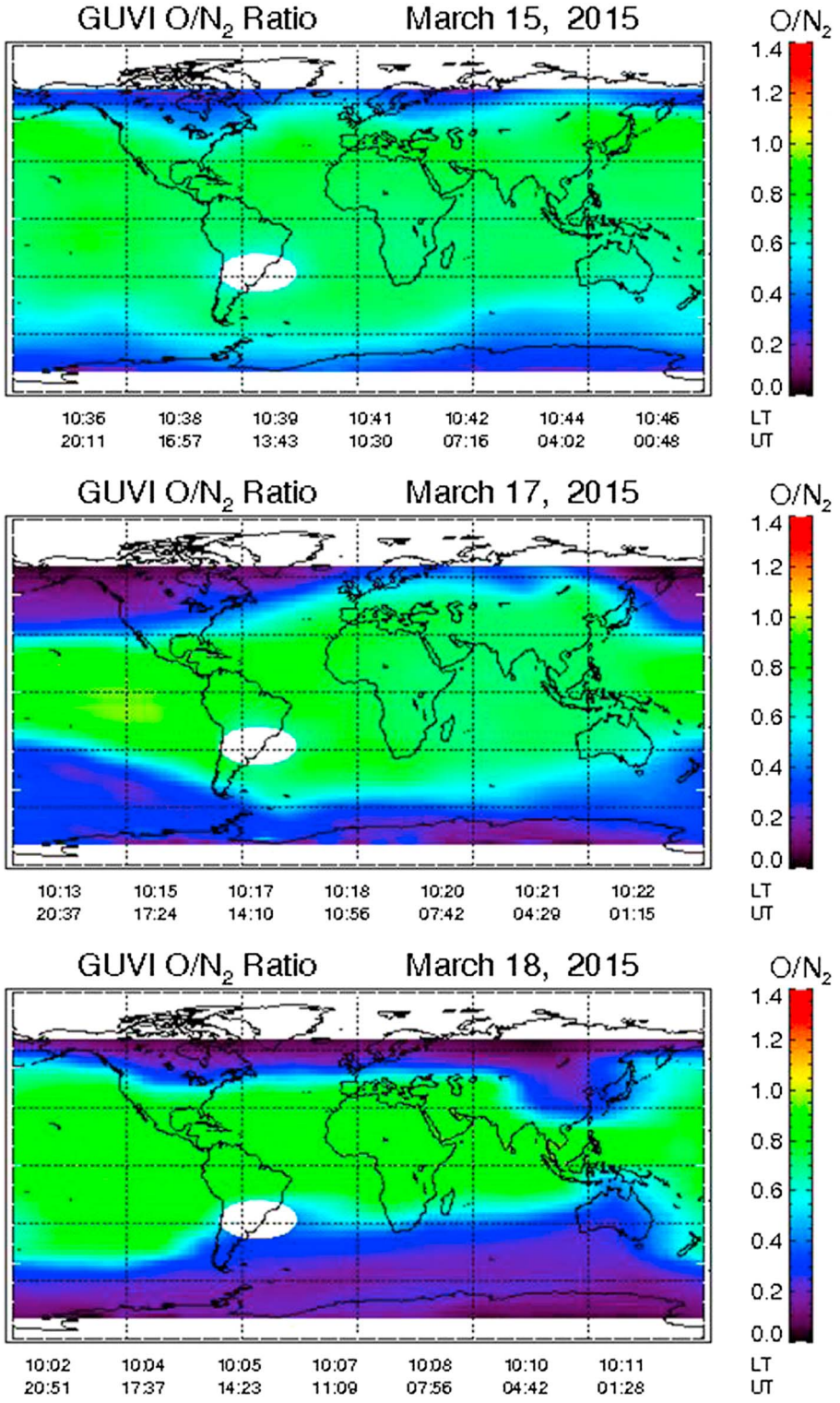


**Figure 10.** The image of global distribution of $O/N_2$ ratio on 15, 17, and 18 March 2015 as measured by TIMED/GUVI satellite. The 17 and 18 March are shown for the main phase and recovery phase of the storm, while 15 March is the nearest quiet day for comparison. The equatorward expansion of lower $O/N_2$ ratio thermospheric composition along the 100°E in Northern Hemisphere and along 120°E in Southern Hemisphere on 18 March may be noted.

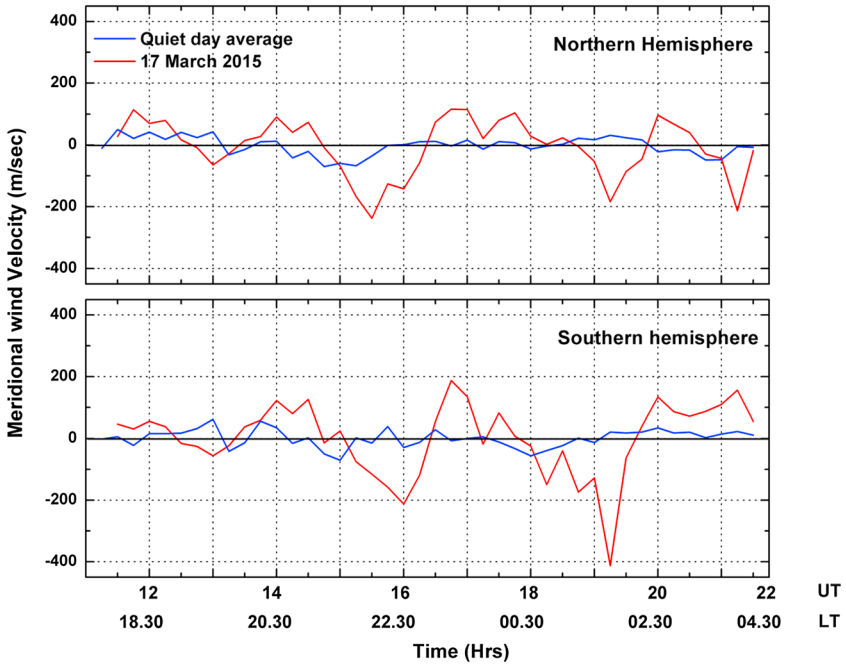


**Figure 11.** The meridional wind velocity along 100°E longitude from SEALION ionosonde network. Positive values indicate poleward velocity.

between low and middle latitudes is likely to be affected by neutral composition disturbances traveling from high latitudes. The thermospheric effects along 100°E are discussed in the next section.

### 4.2. The Thermospheric Response

During strong geomagnetic activity, the density of molecular species relative to atomic oxygen is enhanced in the polar region and these changes expand up to middle and low latitudes [*Prölss*, 1987]. Good correlation of the decrease of $N_mF_2$/TEC (or $F_2$ layer critical frequency) to the directly measured [$O/N_2$] ratio changes has been reported previously [*Prölss and von Zahn*, 1974; *Prölss*, 1987; *Burns et al*., 1991, *Fuller-Rowell et al*., 1994]. The enhanced molecular density and temperature lead to higher recombination rates and cause density depletion in middle and low latitudes. *Astafyeva et al*. [2015] reported large depletion of $O/N_2$ ratio within 100°–130°E during 18 March 2015 which reached the low latitudes in the Asian sector. The GUVI image of 18 March 2015 around 10 LT (Figure 10) indicate a very large decrease in $O/N_2$ ratio (~0.4) in the Northern Hemisphere of 100°E and insignificant thermospheric disturbance in the conjugate Southern Hemisphere as well in the 77°E. According to *Prölss* [1993], the disturbed thermospheric composition or region of enhanced molecular species expands toward the low latitudes in the night sectors when the background condition of lower ion drag and equatorward wind acts favorably. These changes can move into the dayside due to the corotation effect [*Kil et al*., 2011] and consequently affect daytime density. In previous discussion of $h_mF_2$ variations (Figures 3 and 6), it was noted that in the period starting 10:30 UT (17LT) of 17 March, the height variation over the magnetic equator and the off equator stations in 100°E are not simultaneous at all hours and large fluctuations in the ionospheric parameters ($h_mF_2$, $N_mF_2$, and TEC) in the low midlatitudes (Dibrugarh and Cocos Island) as well as at the off magnetic equator stations (Chiang Mai and Kototabang) indicated the propagation of meridional winds or traveling disturbances. The storm-induced joule heating at the polar region set up equatorward meridional winds that add to the quiet time equatorward wind in the premidnight period [*Titheridge*, 1995]. The SEALION network of ionosondes at Chiang Mai, Chumphon, and Kototabang has been used previously to estimate the thermospheric meridional winds [*Maruyama et al*., 2007] with one station (Chumphon) at the geomagnetic equator and the other two stations (Chiang Mai and Kototabang) slightly off the equator at magnetic conjugate points. In this study, we use the virtual height *h'F* obtained by scaling the ionograms of these three stations at 2.5 and 3 MHz during the night of 17 March to estimate the Northern Hemisphere and Southern Hemisphere meridional thermospheric winds

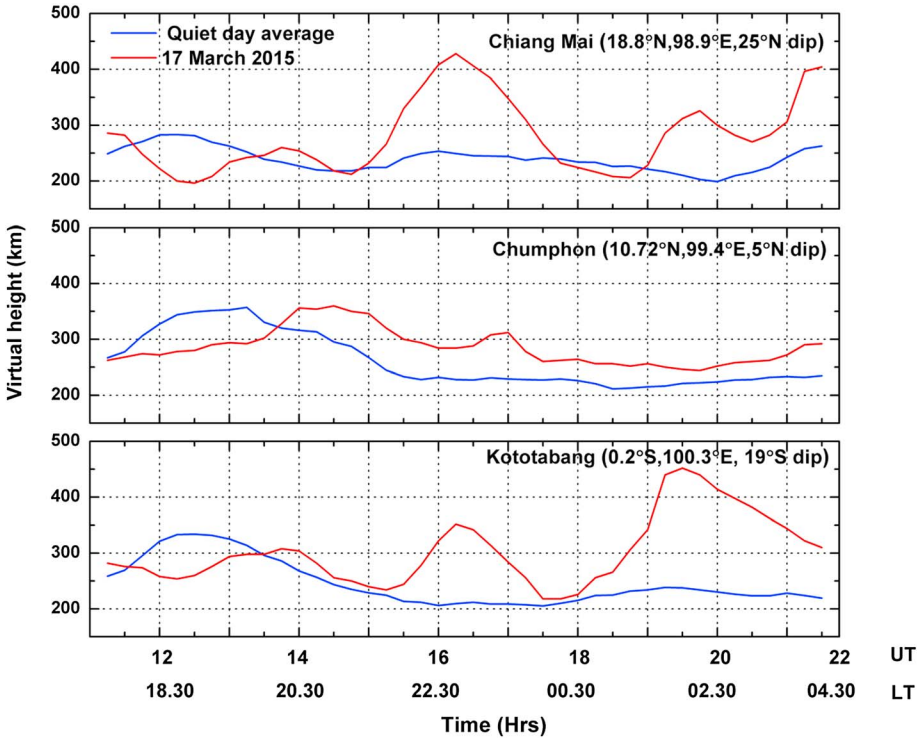


**Figure 12.** The virtual height scaled at 2.5 MHz from the SEALION meridional chain indicating the presence of equatorward meridional wind around 16 UT and 19 UT on 17 March 2015.

following *Krishna Murthy et al*. [1990]. The estimated winds are shown in Figure 11 for the 11:30–23:00 UT period which corresponds to local night time. The top and bottom panels show the Northern Hemisphere and Southern Hemisphere winds, respectively, along with the average quiet day winds for comparison. It is observed that the wind direction fluctuated during the night of 17 March as compared to the quiet day winds. Large equatorward wind surges in the main phase of the storm at around 16 UT and 19 UT can be inferred, which are about 3.5 h after the major substorm development at 12:20 UT and 16 UT as indicated by the *AE* index. The pattern of the winds was also estimated by the method of *Maruyama et al*. [2007] using the model behavior for an equatorial and two magnetic conjugate stations. The virtual heights of the *F* layer over Chiang Mai, Chumphon, and Kototabang scaled from the ionograms at 2.5 MHz are plotted in Figure 12. The relatively higher heights in off equator stations as compared to the equatorial station confirm equatorward wind surge during 16 UT and 19 UT. These height patterns and the periodic variations in the $N_mF_2$/TEC obtained from the spaced ionosonde/TEC observations manifest the traveling ionospheric disturbances (TID) associated with the propagation of traveling atmospheric disturbance (TAD) due to the storm-induced acoustic gravity waves (AGWs). The sequence of the relative heights at the stations located on the magnetic equator and conjugate points also suggest that the TIDs due to the AGW traveling from both the hemispheres interfered in the equator and then passed through to the other hemisphere as suggested by *Hajkowicz and Hunsucker* [1987], *Fuller-Rowell et al*. [1994], and *Balthazor and Moffett* [1997]. The passage of gravity waves can create sporadic $E_s$ layer [*Nygrén et al*., 1990; *Shalimov et al*., 2009], and such a sporadic $E_s$ layer was observed over the low midlatitude station Cocos Island during 15–17 UT on 17 March (not shown) that resulted in complete blanketing of the *F* layer above. The velocity of the TID is estimated using the ground distances between Chiang Mai-Chumphon and Kototabang-Chumphon and is found to be around 430 m/s and 370 m/s for Northern Hemisphere and Southern Hemisphere TIDs, respectively. These speeds are comparable to the equatorward speed of LSTID predicted by *Hajkowicz* [1991] but lower than the speed of 600 m/s predicted by *Fuller-Rowell et al*. [1994]. Therefore, the conjugate hemispherical TEC difference (Dibrugarh-Cocos Island) is likely a thermospheric effect due to asymmetric thermospheric circulations and geographic differences between the stations. The disturbed thermospheric circulation on 18 March is further confirmed by the observation of TID associated with AGW during the daytime over Cocos Island. The

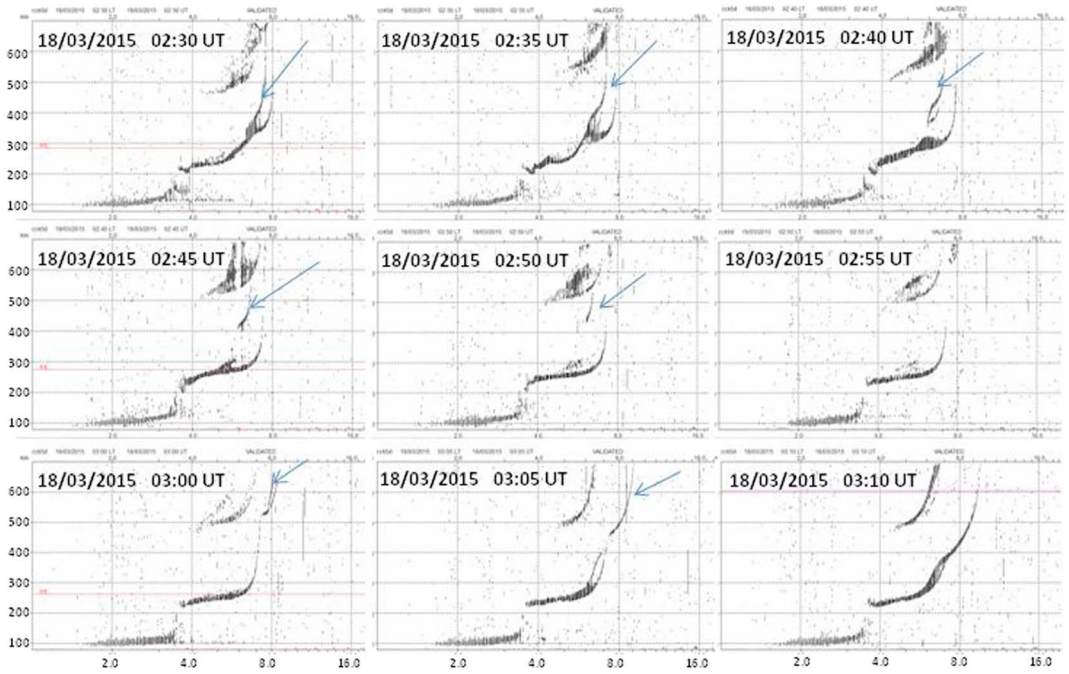


**Figure 13.** The sequence of only ordinary ray trace (O-ray) of ionograms over Cocos Island showing the passage of the traveling ionospheric disturbance (TID). The transient satellite trace due to traveling disturbance is marked by arrow.

ionograms in Cocos Island around 2:30–3:00 UT (~9:30 LT) show an additional upward ledge in the $F_2$ trace which move initially in overhead direction and then move away (Figure 13). The isodensity contours over Cocos Island scaled at 4–7 MHz for the same period (Figure 14) show the downward traveling phase front.

### 4.3. The Ionospheric Response on 17–18 March 2013

The geomagnetic activity indices for the 2013 St. Patrick's Day storm are shown in Figure 15. The storm started at 6:00 UT (SSC), and the first southward excursion of the IMF $B_z$ was observed around 6:20 UT. The storm was less severe than the 2015 storm as minimum *SYM-H* was around −120 nT, and the IMF $B_z$ remained higher than −20 nT throughout. The response of the ionospheric height $h_mF_2$ for the four stations along the 100°E, Chiang Mai, Bac Lieu, Kototabang, and Cocos Island, is shown in Figure 16. Ionosonde data for Chumphon and Dibrugarh for the period of 16–18 March 2013 are not available. The height variation over the equatorial station Bac Lieu on 17 March was modulated by the southward and northward turning of the IMF $B_z$. Increase in $h_mF_2$ around 7 UT due to the first southward turning of IMF $B_z$ and subsequent decrease with northward turning prior to 9 UT is observed. The counter electrojet around 10–11 UT (local afternoon) suggested a westward overshielding electric field, and consequently, the lowest $h_mF_2$ was recorded during this period due to the net drift being downward. Southward IMF $B_z$ around 12 UT (18:30 LT) resulted in large

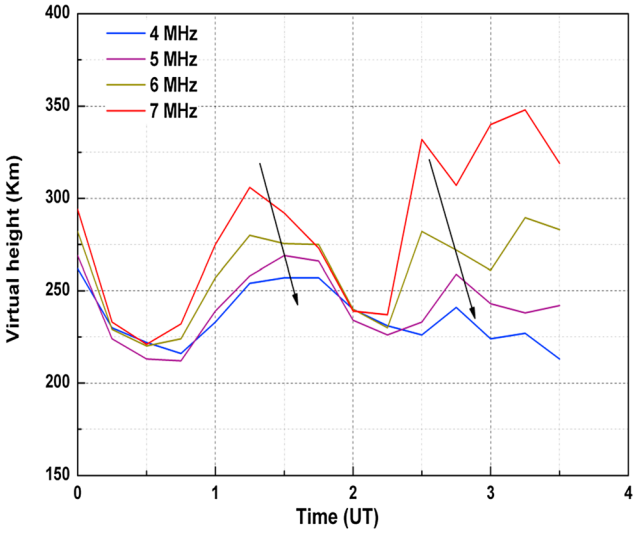


**Figure 14.** The isodensity contours over Cocos Island showing the downward propagating phase during the passage of the TID.

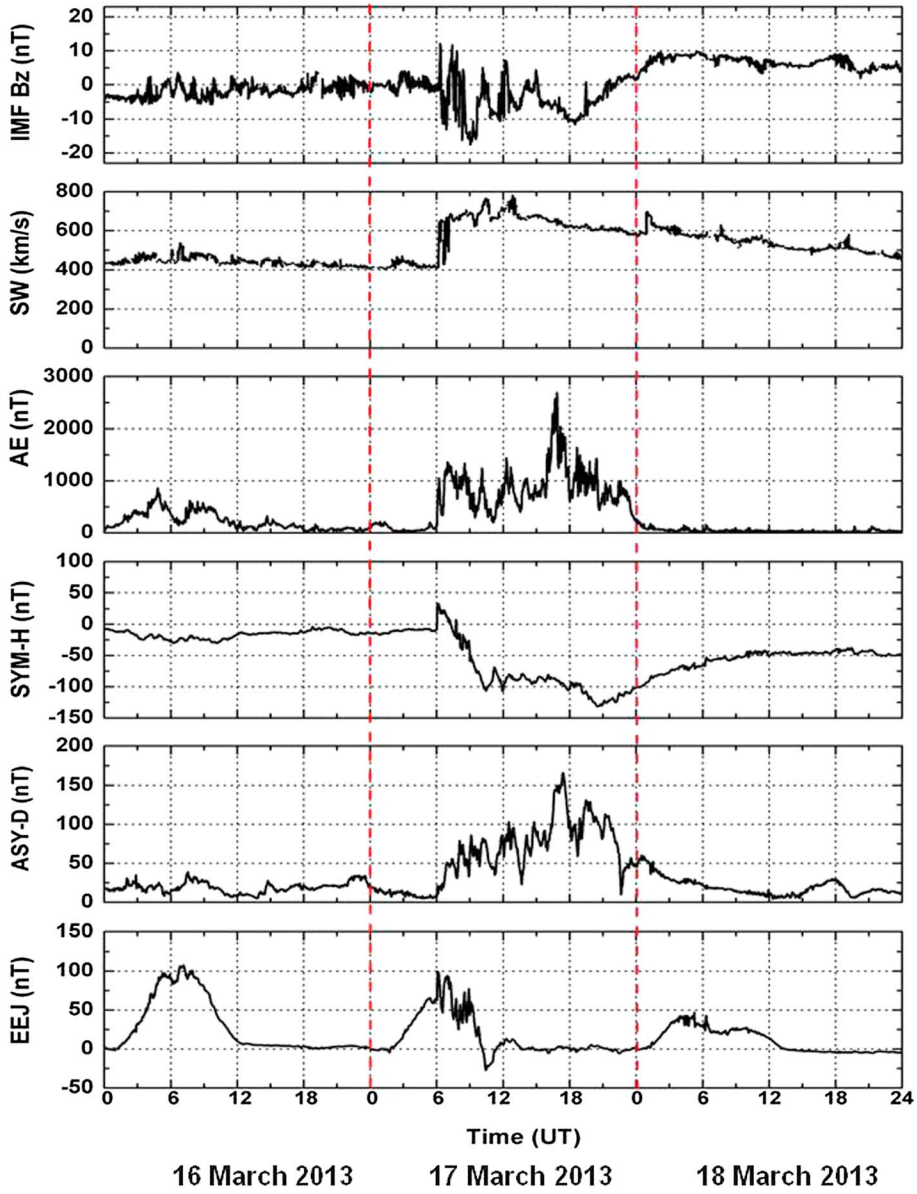


**Figure 15.** The *z* component of interplanetary magnetic field IMF $B_z$, the solar wind speed, the auroral elctrojet index *AE*, the symmetric ring current index *SYM-H*, asymmetric ring current index *ASY-D*, and the equatorial electrojet (EEJ) indices for the period of 16–18 March 2013.

height increase over Chinag Mai and spread *F* over Bac Lieu (Figure 17). L band scintillations were recorded by the GPS receiver in Dibrugarh (Figure 18) but not in Bangalore in the Indian sector. In the postsunset period, the $h_mF_2$ over Bac Lieu was enhanced around 17 UT coinciding with the substorm development (*AE* index). The $h_mF_2$ in Chiang Mai and Kototabang was enhanced around 19 UT without corresponding enhancement over Bac Lieu. Similar to the 2015 storm response, simultaneous height increase but with lower magnitude ($h_mF_2 \sim 500$ km) were observed around 22–23 UT in all stations. This coincided with the local sunrise period and resulted in spread *F* over Bac Lieu. On 18 March, the height variation was almost the same as that on the quiet day with daytime $h_mF_2$ magnitude over Chiang Mai and Kototabang slightly lower than that on the quiet day. The EEJ was very weak on 18 March, but no counter electrojet was observed. The $N_mF_2$ measurements over Chiang Mai, Bac Lieu, Kototabang, and Cocos Island are shown in Figure 19. The $N_mF_2$ over equatorial region was higher than the quiet day values in the local afternoon period and showed a peak around 12 UT. In the postsunset period, the maximum diurnal $N_mF_2$ over Kototabang was recorded around 15 UT (21 LT) with

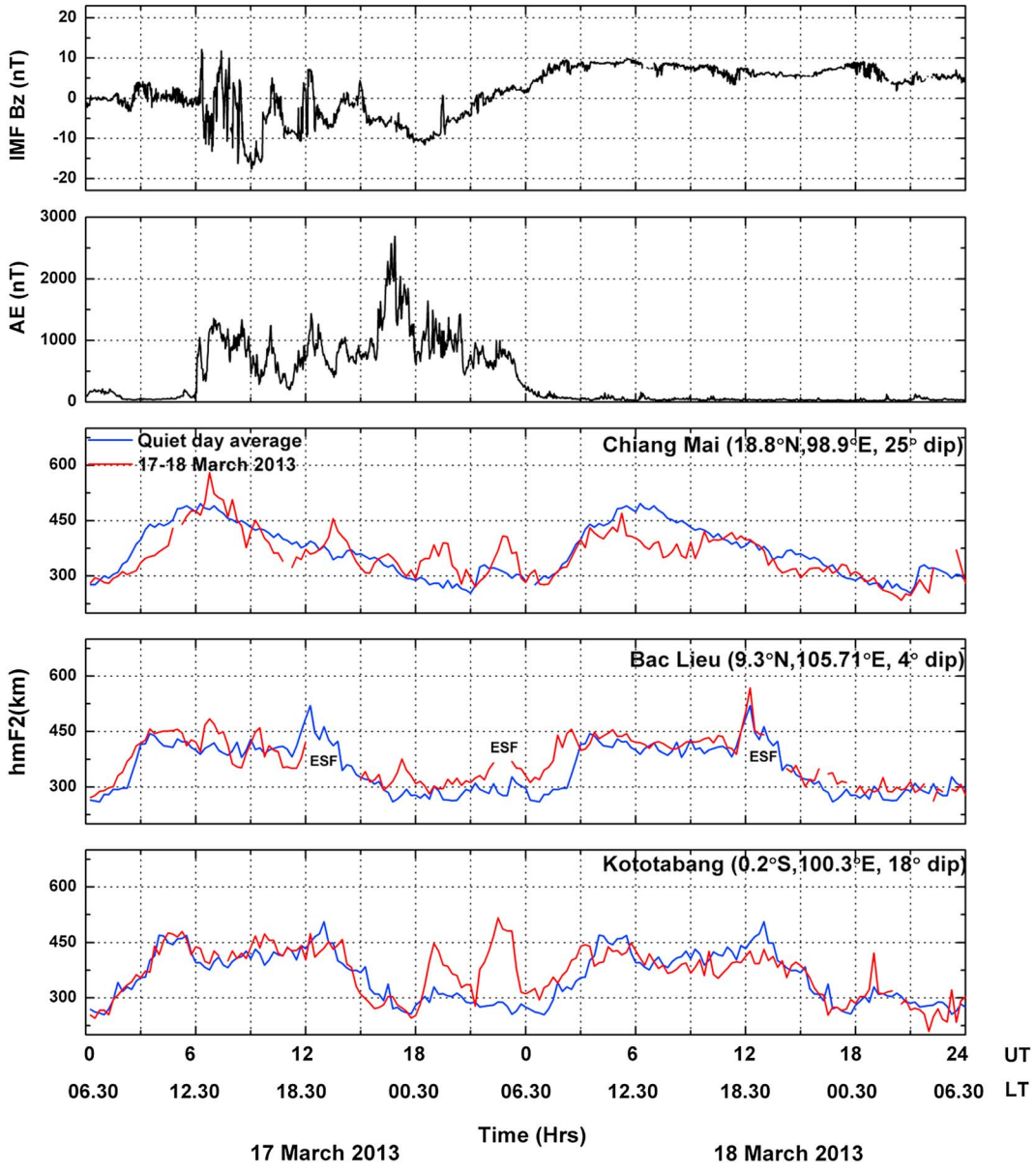


**Figure 16.** The variation of $F_2$ layer height $h_mF_2$ in the 100°E longitude on 17 and 18 March 2013.

similar but lower amplitude enhancements over Bac Lieu and Chiang Mai. In Cocos Island, the $N_mF_2$ on the local evening of 17 March to early morning period of 18 March was lower than the equatorial values, and therefore, the equatorial anomaly was inhibited in the local nighttime. On 18 March, the $N_mF_2$ was enhanced (depleted) in the equatorial stations (low latitude) as compared to the quiet day values. In low-latitude station Cocos Island, the daytime $N_mF_2$ reduction was severe (>66%) as compared the $N_mF_2$ enhancements in equatorial stations (~33%). The TEC for the 100°E longitude stations Dibrugarh, Port Blair, and Cocos Island and the 77°E longitude stations Lucknow and Bangalore are shown in Figure 20. Significant TEC enhancements over Dibrugarh and Cocos Island can be observed after storm commencement on 17 March in contrast to Lucknow in the Indian sector. The TEC in the equatorial stations, Port Blair and Bangalore, was enhanced in the local afternoon sector, whereas the TEC in Dibrugarh and Lucknow exhibited rapid fluctuations. Dibrugarh recorded a secondary peak in the postsunset period, whereas Cocos Island on Southern Hemisphere showed flatter TEC. The disturbed day TEC in the postsunset period was higher in the equatorial region as compared to the low-latitude region indicating the inhibition of EIA in both longitudes. TEC enhancements (depletion) are observed in the equatorial region (low latitude) indicating positive (negative) storm effect in the recovery phase. Therefore, the TEC mirrored the

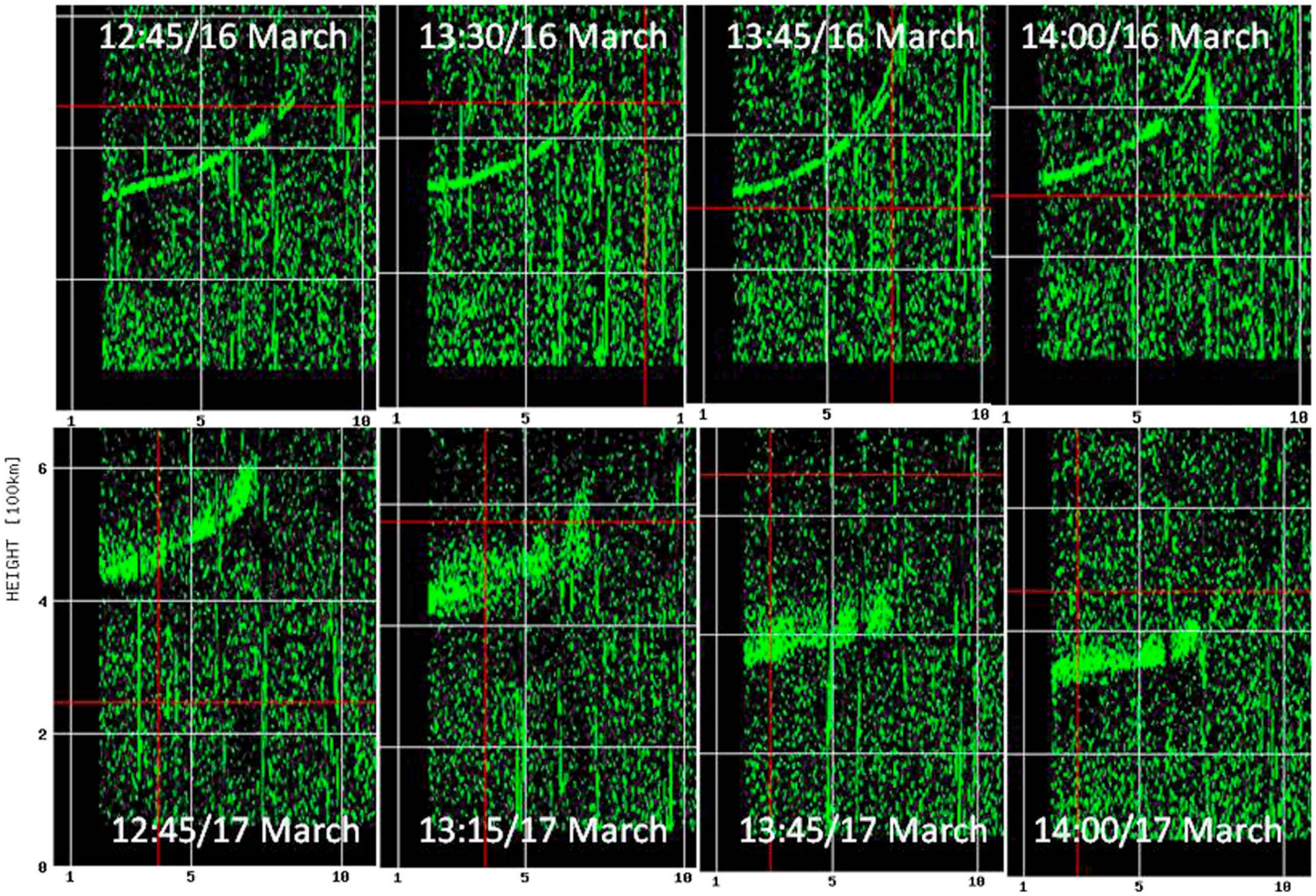


**Figure 17.** The ionograms over Bac Lieu showing the postsunset $F_2$ layer on a 16 March and spread $F$ during 17 March 2013.

behavior of the $N_mF_2$. TEC enhancements of about 35% in equatorial stations and TEC depletion of about 20%, 40%, and 66% in Dibrugarh, Lucknow, and Cocos Island, respectively, were observed. In contrast to the storm response on St. Patrick's Day of 2015, in 2013, the negative effect is stronger in the Southern Hemisphere station Cocos Island relative to the Northern Hemisphere station Dibrugarh. On the night of 17 March, TEC over Dibrugarh is almost same as the quiet day TEC, whereas the TEC over Cocos Island is lower than quiet time values. On 18 March, the TEC in Cocos Island starts to decrease after 4 UT (10:30 LT), whereas Dibrugarh and Lucknow TEC decreases only after 8 UT (12:30 LT). On 18 March, the EEJ was weaker as compared to that on 16 March and can explain the equatorial enhancement and the postnoon low-latitude depletion as due to the weakening of the plasma fountain/EIA. The severe TEC and $N_mF_2$ (~58%) depletion over Cocos Island on 18 March coincided with the decrease of $O/N_2$ ratio to ~ 0.6 in the forenoon period (~10 LT) of 100°–130°E in the Southern Hemisphere as observed from TIMED/GUVI image (Figure 21). It is interesting to note that during 18 March 2015, such severe $O/N_2$ change in the forenoon was observed for the Northern Hemisphere low latitude and coincided with severe negative effect over Dibrugarh and Kohima. The longitudinal expansion of the thermospheric disturbance seems to be limited to a narrow belt around 100–130°E and the Indian sector was less affected in the forenoon period. This behavior is similar to the 2015 storm response and indicative of the sharp longitudinal variability of the storm time dynamics. Therefore, even though the GUVI measurements are for a very brief period in the forenoon, it is indicative of the level of negative storm effect during the peak daytime hours.

To estimate the neutral meridional circulations on the night of 17 March, the virtual heights scaled at 2.5 MHz from ionograms over Bac Lieu, Chiang Mai, and Kototabang are shown in Figure 22 for the 11:30–23:30 UT

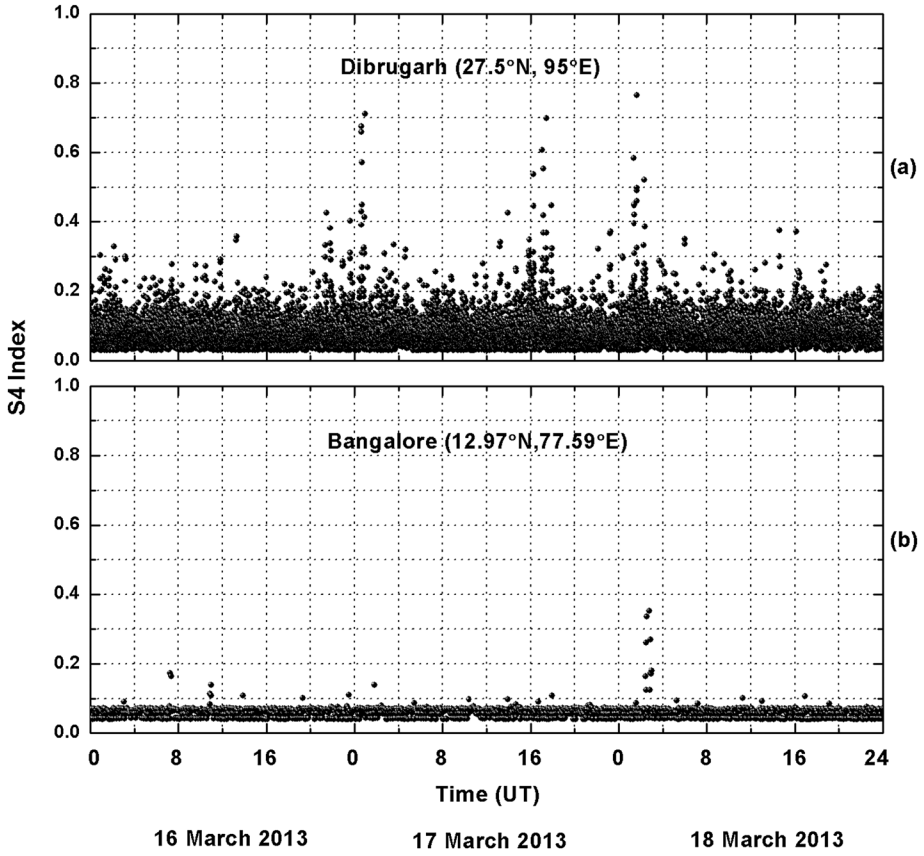


**Figure 18.** The S4 index for 16–18 March 2013 showing the scintillations over Dibrugarh in the local evening of 17 March. The elevation angle is cutoff at 30°.

hours. Chiang Mai and Kototabang are almost at the same meridian (~99–100°E), while Bac Lieu is at slightly different meridian (~106°E). Due to the data unavailability over 99°E meridian station Chumphon, the meridional winds could not be calculated and the height variations in Figure 22 are used as indicator of meridional winds in this sector. The evening height increase related to the PRE is observed over Bac Lieu but not in the other two equatorial stations. The height enhancement around 19 UT over Chiang Mai and Kototabang and the absence over Bac Lieu suggest that these changes are due to the thermospheric meridional winds. The variations in the nighttime $N_mF_2$ (Figure 19) can be ascribed to the height variations. The simultaneous height enhancement around 22:30 UT which corresponds to the sunrise period in local time could be related to the PPEF and/or disturbance dynamo drift [*Scherliess and Fejer*, 1997].

### 4.4. The Comparison of the Ionospheric Response in 2013 and 2015

The ionospheric response to the 17–18 March geomagnetic storms in 2013 and 2015 are similar in the following aspects:

1. The southward (northward) turning of the IMF $B_z$ was reflected as increase (decrease) of the $h_mF_2$ and fluctuations in $N_mF_2$ and TEC. During the main phase of both the storm, significant fluctuations in the equatorial zonal electric field due to the penetration of magnetospheric convective electric fields could be inferred.
2. The equatorial $N_mF_2$/TEC during both the storms was enhanced in the sunset period, whereas the low-latitude $N_mF_2$/TEC was depleted in the postsunset sector, thereby indicating the inhibition of the nighttime EIA.
3. Large nighttime variations in the $h_mF_2$, $N_mF_2$, and TEC were observed in the 100°E meridian on storm day due to traveling disturbances.
4. Sharp height increase and ESF was observed during the sunrise period of 18 March. The early morning height enhancements were larger in 2015 as compared to that in 2013. To investigate the cause of this height enhancement, the empirical vertical drift model after *Scherliess and Fejer* [1997] was used to obtain

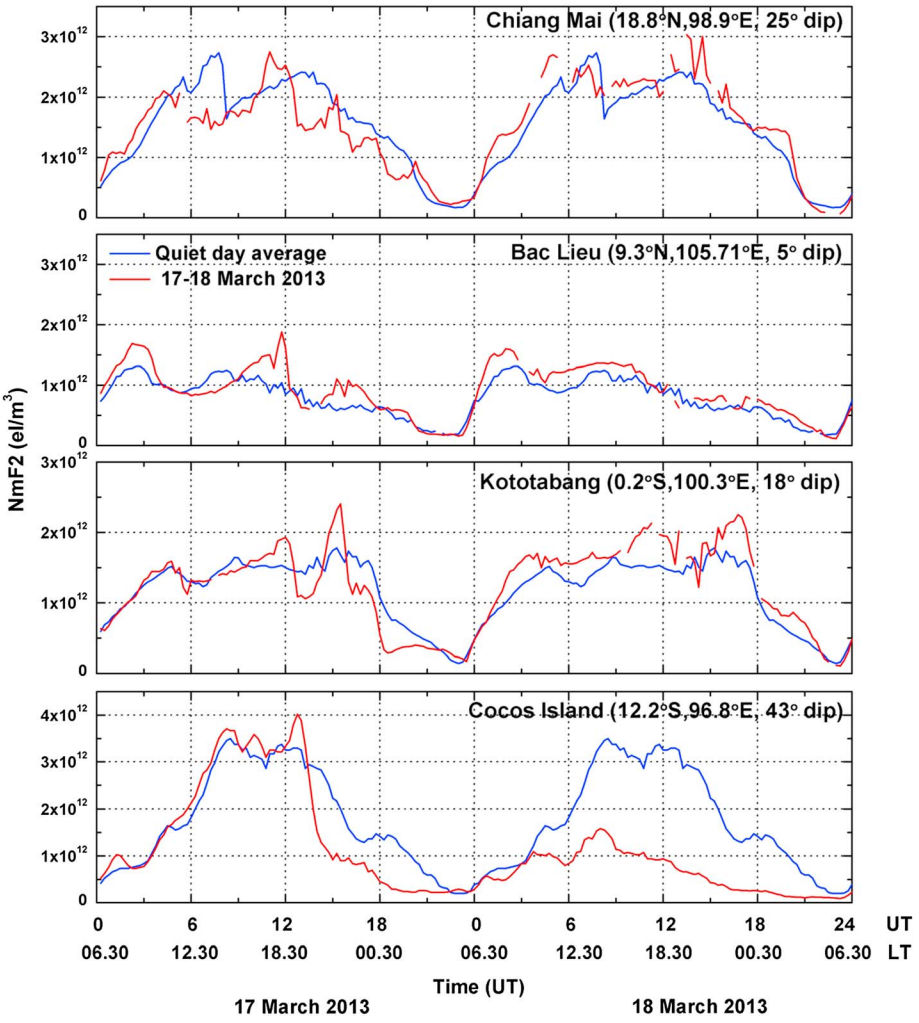


**Figure 19.** The variation of $F_2$ layer peak density $N_mF_2$ in the 100°E on 17 and 18 March 2013. The scales for the equatorial and low-latitude station are different to highlight the fluctuations.

the vertical drift on 17 March. The model uses the *AE* index and the $F_{10.7}$ flux data as input and provides the quiet time drift, PPEF, and disturbance dynamo drift and the total drift. The drift due to the PPEF and the disturbance dynamo electric field and the total drift (quiet time + disturbed drift) are shown in Figure 23 (left column). The model predicted very high upward vertical drift during the local sunrise hours for both the storm with higher amplitude in 2015 (~40 m/s) which is supported by much higher measured $h_mF_2$ during 2015 (~700 km; Figure 3) as compared to 2013 (~500 km; Figure 16). In 2015, the model-predicted vertical drift in the sunrise period of 18 March is higher than the drift during evening PRE of 17 March. The vertical drift estimated from the rate of change of nighttime virtual height (*h'F*) over Bac Lieu in 2013 and Chumphon in 2015 are compared with the model drift in Figure 23 (right column). The observed vertical drift during sunrise of 18 March 2015 (2013) is larger than (same as) drift during sunset period of 17 March 2015 (2013). The observed drift during sunrise is slightly delayed and larger (in 2013) than the model drift. Such unusually large upward drift resulted in the irregularity development and ESF during sunrise period in both the storms.

In spite of this generally similar response of the ionosphere during the St. Patrick's Day storms of 2013 and 2015, the following subtle differences were noted:

1. The northward (southward) direction of the IMF $B_z$ during the sunset period of 17 March 2015 (2013) inhibited (enhanced) the prereversal enhancement (PRE) in zonal electric field and consequent irregularity formation.

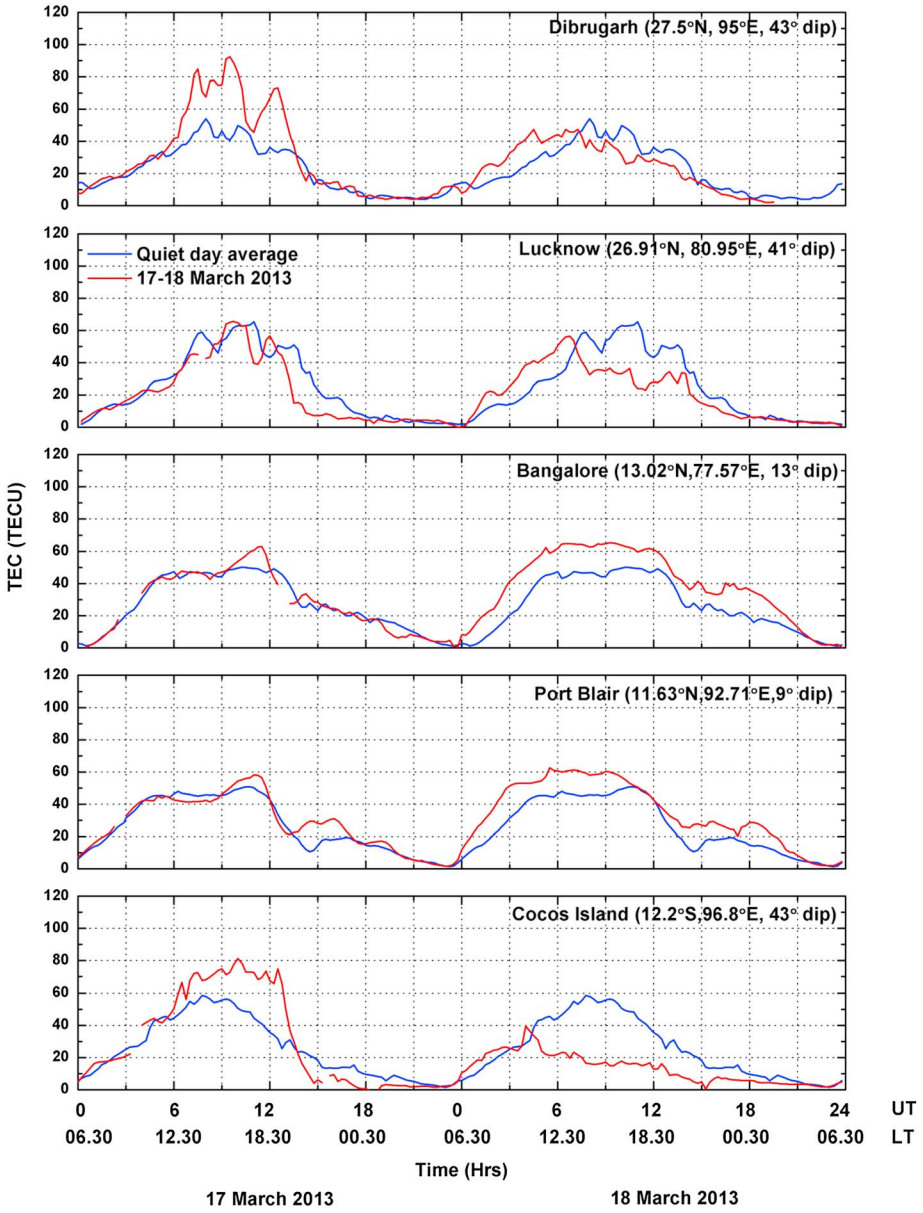


**Figure 20.** The variation of TEC in the 100°E longitude on 17 and 18 March 2013 and comparison with TEC in 77°E longitude.

2. Postsunset irregularities caused ESF and scintillations in the 100°E, but no scintillations were observed in the 77°E during the evening of 17 March 2013. The response was reversed during the evening of 17 March 2015 when ESF and L band amplitude scintillations were observed over the Indian sector but not in the 100°E sector. These longitudinal differences are attributed to the local time variation of electrodynamic processes with the changing direction of IMF $B_z$.
3. The EIA was weakened on 18 March 2013, whereas it was completely inhibited on 18 March 2015.
4. The negative (positive) effect of the storm in the recovery phase of the storm (18 March) in low-latitude (equatorial) region was stronger in 2015 as compared to 2013. The negative effect of the storm was marked by longitudinal and hemispherical asymmetry. In 2013, the $O/N_2$ depletions around 10 LT and the negative storm effect in TEC were severe in the Southern Hemisphere station Cocos Island as compared to the moderate effect in the Northern Hemisphere conjugate station Dibrugarh. The opposite thermospheric-ionospheric response was observed in 2015 as the forenoon compositional change and TEC depletions were stronger over Dibrugarh. The severe negative storm effect over Dibrugarh in

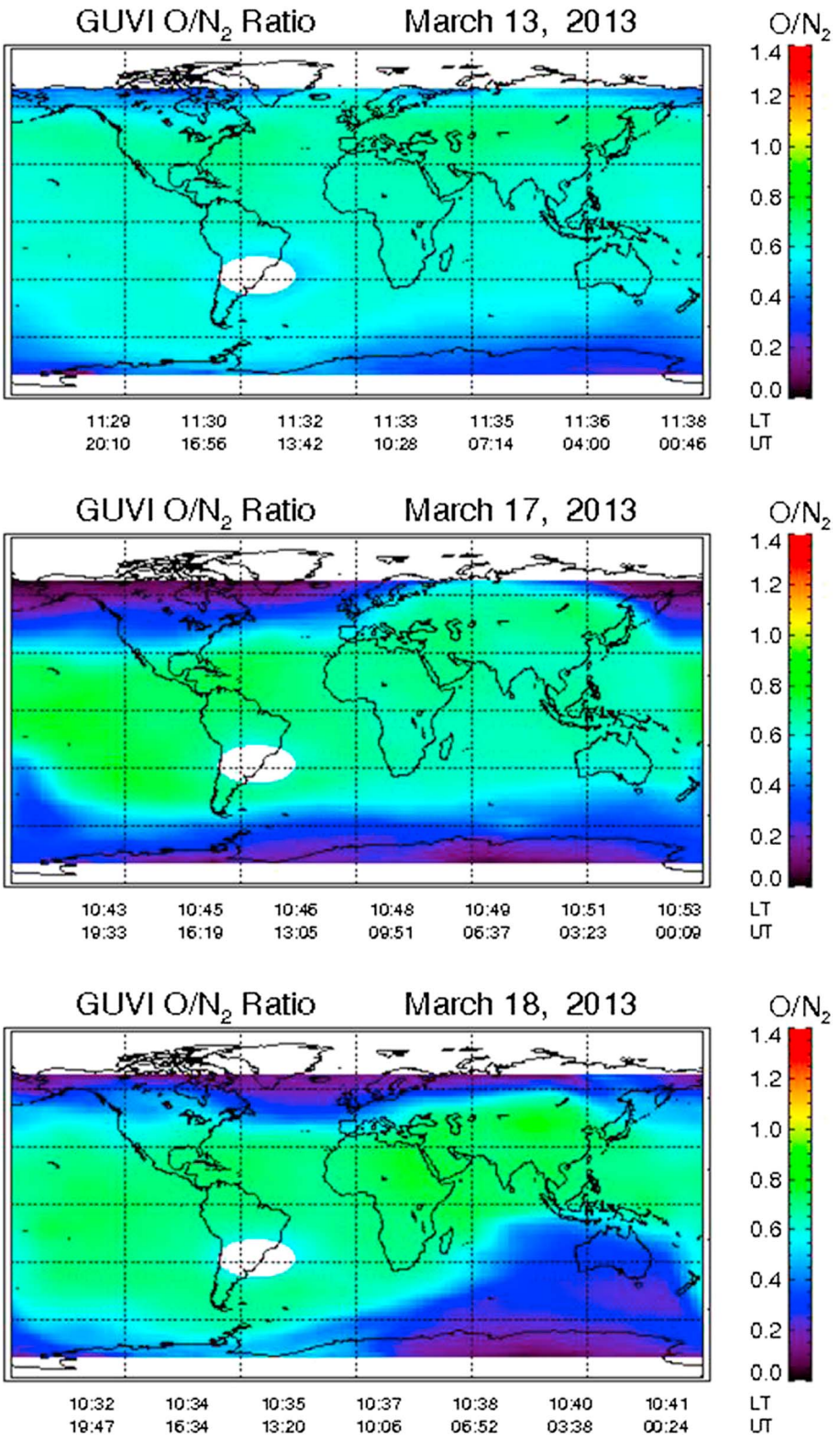


**Figure 21.** The image of global distribution of $O/N_2$ ratio on 13, 17, and 18 March 2013 as measured by TIMED/GUVI satellite. The image of 17 and 18 March show the main phase and recovery phase of the storm, while 13 March is the nearest quiet day for comparison. The equatorward expansion of lower $O/N_2$ ratio thermospheric composition can be noted around 100–120°E in Southern Hemisphere on 18 March. In contrast no such expansion to northern low latitude is observed.

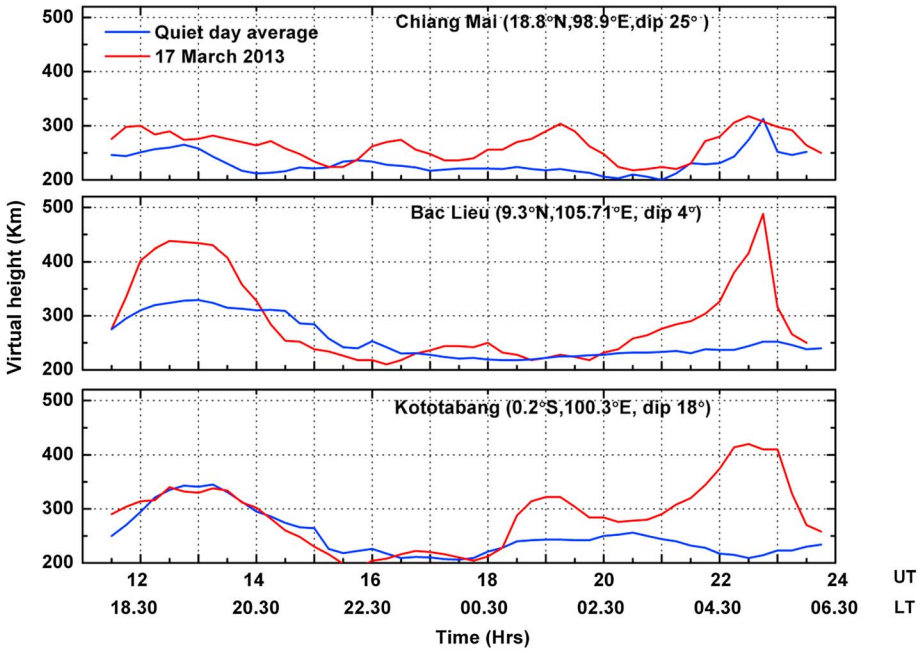


**Figure 22.** The nighttime virtual height at 2.5 MHz indicating the presence of equatorward meridional winds during 19 UT (01:30 LT) of 17 March 2013.

2015 cannot be attributed to the electrodynamics alone as the effect was much stronger than the corresponding positive (negative) effect at the equator (conjugate location) and preceded the equatorial anomaly development. The negative effect in Kohima which is closer to the EIA crest was also comparatively less severe than that in Dibrugarh. Similarly, the negative effect over Cocos Island in 2013 was much stronger than the corresponding enhancement (depletion) over equatorial region (Dibrugarh). In both

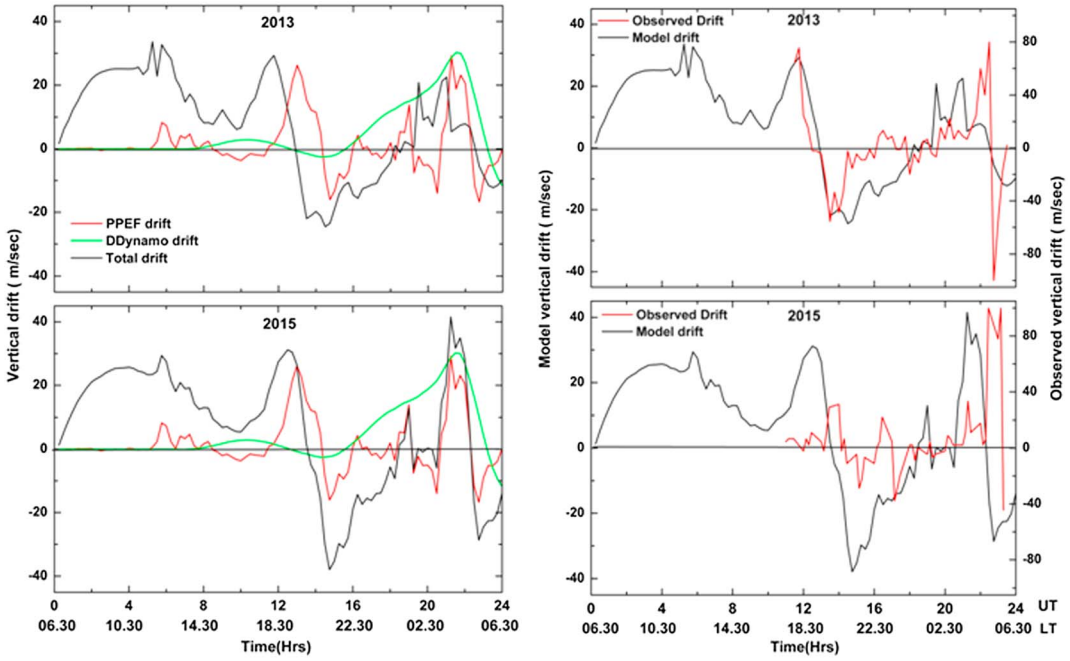


**Figure 23.** (left column) The variation of model vertical drift due to the PPEF and the Disturbance Dynamo and the total (quiet + disturbance) drift on 17 March. (right column) The comparison of the model drift with the observed drift over Bac Lieu (in 2013) and Chumphon (in 2015) estimated from the rate of change of night time virtual height.

these cases, thermospheric composition played a significant role as hinted by the $O/N_2$ measurement in the forenoon period. Therefore, the severe negative storm effect in Dibrugarh/Kohima in 2015 and in Cocos Island in 2013 is attributed to combined effect of electrodynamic and thermospheric perturbations.

5. The longitudinal asymmetry of ionospheric response vis-a-vis the negative effect is observed. The longitudinal differences in the disturbance dynamo electric fields, thermospheric circulation, and magnetic pole offset as well as the unknown longitudinal variation in the auroral energy deposition may contribute toward the longitudinal asymmetry.
6. Significant thermospheric effect in the 100°E longitude sector lasted till 18 March 2015 as shown by TID over Cocos Island.

## 5. Conclusions

The ionospheric response to the St. Patrick's Day storms of 2013 and 2015 along the 100°E meridian is presented using multi-instrument data from magnetically near conjugate stations from middle to low and equatorial latitudes. The observations are also compared with that in the Indian sector. The conclusions can be summarized as below:

1. The ebb and flow of the equatorial plasma fountain induced by the perturbation of zonal electric field causes appreciable density and electron content variation in the equatorial anomaly region.
2. The direction of the IMF $B_z$ during the sunset period is pivotal to the evening equatorial electrodynamics —either enhancing or inhibiting the irregularity formation.
3. The storm-induced upward vertical drift at sunrise can be larger than the drift during evening PRE. This lead to sharp height increase and consequently enable equatorial irregularity formation (spread *F*).
4. The negative effect in the low latitude during the recovery phase of the storm may be attributed to the EIA inhibition as well as thermospheric composition modification. The expansion of thermospheric compositional disturbance or $O/N_2$ suppression region to the low latitudes could cause severe negative storm effect (>50%) when it overlap with the EIA inhibition region.
5. The hemispherical asymmetry of the negative storm response is contributed mainly by the asymmetric expansion of the disturbed thermospheric composition, whereas the longitudinal asymmetry may be attributed to electrodynamic as well as thermospheric processes.

**Acknowledgments**

The study is sponsored by the SERB, Department of Science and Technology, Government of India through the grant SB/S4/As-127/2013. The authors are grateful to ACE SWEPAM for providing the IMF $B_z$ data. The authors also acknowledge the NASA/GSFC's Space Physics data facility's OMNIWeb for the Wind satellite IMF $B_z$, solar wind, *AE*, and *ASY-D* index data. For *SYM-H*, we are thankful to World Data Center for Geomagnetism, Kyoto University. The authors would like thank the Indian Institute of Geomagnetism (IIG), Mumbai, for providing the EEJ data. The GUVI data used here are provided through support from the NASA MO&DA program. The GUVI instrument was designed and built by The Aerospace Corporation and The John Hopkins University. The Principal Investigator is Andrew B. Christensen and the Chief Scientist and the co-PI is Larry J. Paxton. The authors would like to thank Ludger Scherliess for providing the empirical vertical drift model and kind suggestions. Rumajyori Hzarika and Geetashri Kakoti are grateful to DST, Government of India, for providing the fellowship under the above mentioned grant. The work of D.Chakrabarty is supported by the Department of Space, Government of India. The ionospheric data for Dibrugarh, Kohima, Ahmedabad, Cocos Island, and the SEALION are available with the authors.

## References

Abdu, M. A. (2001), Outstanding problems in the equatorial ionosphere-thermosphere electrodynamics relevant to spread *F*, *J. Atmos. Sol. Terr. Phys.*, *63*, 869–884, doi:10.1016/S1364-6826(00)00201-7.

Acharya, R., N. Nagori, N. Jain, S. Sunda, M. R. Sivaraman, and K. Bandyopadhyay (2007), Ionospheric studies for the implementation of GAGAN, *Indian J. Radio Space Phys.*, *36*(5), 394–404.

Astafyeva, E., I. Zakharenkova, and M. Förster (2015), Ionospheric response to the 2015 St. Patrick's Day storm: A global multi-instrumental overview, *J. Geophys. Res. Space Physics*, *120*, 9023–9037, doi:10.1002/2015JA021629.

Balan, N., and G. J. Bailey (1995), Equatorial plasma fountain and its effects: Possibility of an additional layer, *J. Geophys. Res.*, *100*, 21,421–21,432, doi:10.1029/95JA01555.

Balan, N., et al. (2011), A statistical study of the response of the dayside equatorial $F_2$ layer to the main phase of intense geomagnetic storms as an indicator of penetration electric field, *J. Geophys. Res.*, *116*, A03323, doi:10.1029/2010JA016001.

Balthazor, R. L., and R. J. Moffett (1997), A study of atmospheric gravity waves and travelling ionospheric disturbances at equatorial latitudes, *Ann. Geophys.*, *15*(8), 1048–1056, doi:10.1007/s00585-997-1048-4.

Basu, S., J. McClure, S. Basu, W. Hanson, and J. Aarons (1980), Coordinated study of equatorial scintillation and in situ and radar observations of nighttime *F* region irregularities, *J. Geophys. Res.*, *85*, 5119–5130, doi:10.1029/JA085iA10p05119.

Basu, S., et al. (1996), Scintillations, plasma drifts, and neutral winds in the equatorial ionosphere after sunset, *J. Geophys. Res.*, *101*, 26,795–26,809, doi:10.1029/96JA00760.

Bhuyan, P. K., and R. Hazarika (2012), GPS TEC near the crest of the EIA at 95°E during the ascending half of solar cycle 24 and comparison with IRI simulations, *Adv. Space Res.*, *52*, 1247–1260, doi:10.1016/j.asr.2013.06.029.

Bhuyan, P. K., and R. R. Borah (2007), TEC derived from GPS network in India and comparison with the IRI, *Adv. Space Res.*, *39*(5), 830–840, doi:10.1016/j.asr.2006.12.042.

Blanc, M., and A. Richmond (1980), The ionospheric disturbance dynamo, *J. Geophys. Res.*, *85*, 1669–1686, doi:10.1029/JA085iA04p01669.

Burns, A. G., T. L. Killeen, and R. G. Robie (1991), A simulation of thermospheric composition changes during an impulse storm, *J. Geophys. Res.*, *96*, 14,153–14,167, doi:10.1029/91JA00678.

Chakrabarty, S. K., and R. Hajra (2009), Electrojet control of ambient ionization near the crest of the equatorial anomaly in the Indian zone, *Ann. Geophys.*, *27*, 93–105, doi:10.5194/angeo-27-93-2009.

Chandra, H., and R. G. Rastogi (1974), Geomagnetic storm effects on ionospheric drifts and the equatorial Es over the magnetic equator, *Ind. J. Radio Space Phys.*, *3*, 332–336.

DasGupta, A., S. Basu, J. Aarons, J. A. Klobuchar, S. Basu, and A. Bushby (1983), VHF amplitude scintillations and associated electron content depletions as observed at Arequipa, Peru, *J. Atmos. Sol. Terr. Phys.*, *45*, 15–26, doi:10.1016/S0021-9169(83)80003-8.

England, S. L., S. Maus, T. J. Immel, and S. B. Mende (2006), Longitudinal variation of the *E*-region electric fields caused by atmospheric tides, *Geophys. Res. Lett.*, *33*, L21105, doi:10.1029/2006GL027465.
Fejer, B. G., and J. T. Emmert (2003), Low-latitude ionospheric disturbance electric field effects during the recovery phase of the19–21 October 1998 magnetic storm, *J. Geophys. Res.*, *108*(A12), 1454, doi:10.1029/2003JA010190.
Fejer, B. G., L. Scherliess, and E. R. de Paula (1999), Effects of the vertical plasma drift velocity on the generation and evolution of equatorial spread *F*, *J. Geophys. Res.*, *104*, 19,859–19,869, doi:10.1029/1999JA900271.
Fesen, C. G., G. Crowley, and R. G. Roble (1989), Ionospheric effects at low latitudes during the March 22, 1979, geomagnetic storm, *J. Geophys. Res.*, *94*, 5405–5417, doi:10.1029/JA094iA05p05405.
Field, P. R., and H. Rishbeth (1997), The response of the ionospheric $F_2$ layer to geomagnetic activity: an analysis of worldwide data, *J. Atmos. Sol. Terr. Phys.*, *59*(2), 163–180, doi:10.1016/S1364-6826(96)00085-5.
Field, P. R., H. Rishbeth, R. J. Moffett, D. W. Wenden, T. J. Fuller-Rowell, G. H. Millward, A. D. Aylward (1998), Modelling composition changes in F-layer storms, *J. Atmos. Sol. Terr. Phys.*, *60*(5), 523–543, doi:10.1016/S1364-6826(97)00074-6.
Fuller-Rowell, T. J., M. V. Codrescu, R. J. Moffett, and S. Quegan (1994), Response of the thermosphere and ionosphere to geomagnetic storms, *J. Geophys. Res.*, *99*, 3893–3914, doi:10.1029/93JA02015.
Hajkowicz, L. A. (1991), Auroral electrojet effect on the global occurrence pattern of large scale travelling ionospheric disturbances, *Planet. Space Sci.*, *39*(8), 1189–1196, doi:10.1016/0032-0633(91)90170-F.
Hajkowicz, L. A., and R. D. Hunsucker (1987), A simultaneous observation of large-scale periodic TIDs in both hemispheres following an onset of auroral disturbances, *Planet. Space Sci.*, *35*, 785–791, doi:10.1016/0032-0633(87)90038-9.
Immel, T. J., E. Sagawa, S. L. England, S. B. Henderson, M. E. Hagan, S. B. Mende, H. U. Frey, C. M. Swenson, and L. J. Paxton (2006), The control of equatorial ionospheric morphology by atmospheric tides, *Geophys. Res. Lett.*, *33*, L15108, doi:10.1029/2006GL026161.
Kamide, Y., R. L. McPherron, W. D. Gonzalez, D. C. Hamilton, H. S. Hudson, J. A. Joselyn, S. W. Kahler, L. R. Lyons, H. Lundstedt, and E. Szuszczewicz (1997), Magnetic storms: Current understanding and outstanding questions, in *Magnetic Storms*, edited by B. T. Tsurutani, et al., pp. 1–19, AGU, Washington, D. C., doi:10.1029/GM098p0001.
Kamide, Y., et al. (1998), Current understanding of magnetic storms: Storm-substorm relationships, *J. Geophys. Res.*, *103*, 17,705–17,728, doi:10.1029/98JA01426.
Kelley, M. C., B. G. Fejer, and C. A. Gonzales (1979), An explanation for anomalous equatorial ionospheric electric fields associated with a northward turning of the interplanetary magnetic field, *Geophys. Res. Lett.*, *6*, 301–304, doi:10.1029/GL006i004p00301.
Kelley, M. C., J. J. Makela, O. de La Beaujardière, and J. Retterer (2011), Convective ionospheric storms: A review, *Rev. Geophys.*, *49*, RG2003, doi:10.1029/2010RG000340.
Kikuchi, T., H. Lühr, T. Kitamura, O. Saka, and K. Schlegel (1996), Direct penetration of the polar electric field to the equator during a DP 2 event as detected by the auroral and equatorial magnetometer chains and the EISCAT radar, *J. Geophys. Res.*, *101*, 17,161–17,173, doi:10.1029/96JA01299.
Kikuchi, T., H. Lühr, K. Schlegel, H. Tachihara, M. Shinohara, and T. I. Kitamura (2000), Penetration of auroral electric fields to the equator during a substorm, *J. Geophys. Res.*, *105*, 23,251–23,261, doi:10.1029/2000JA900016.
Kikuchi, T., Y. Ebihara, K. K. Hashimoto, R. Kataoka, T. Hori, S. Watari, and N. Nishitani (2010), Penetration of the convection and overshielding electric fields to the equatorial ionosphere during a quasiperiodic *DP* 2 geomagnetic fluctuation event, *J. Geophys. Res.*, *115*, A05209, doi:10.1029/2008JA013948.
Kil, H., E. R. Talaat, S. J. Oh, L. J. Paxton, S. L. England, and S. Y. Su (2008), Wave structures of the plasma density and vertical $E \times B$ drift in low-latitude *F* region, *J. Geophys. Res.*, *113*, A09312, doi:10.1029/2008JA013106.
Kil, H., L. J. Paxton, K.-H. Kim, S. Park, Y. Zhang, and S. J. Oh (2011), Temporal and spatial components in the storm time ionospheric disturbances, *J. Geophys. Res.*, *116*, A11315, doi:10.1029/2011JA016750.
Krishna Murthy, B. V., S. S. Hari, and V. V. Somayajulu (1990), Nighttime equatorial thermospheric meridional winds from ionospheric h'F data, *J. Geophys. Res.*, *95*, 4307–4310, doi:10.1029/JA095iA04p04307.
Le, G., et al. (2016), Magnetopause erosion during the 17 March 2015 magnetic storm: Combined field-aligned currents, auroral oval, and magnetopause observations, *Geophys. Res. Lett.*, *43*, 2396–2404, doi:10.1002/2016GL068257.
Liou, K., P. T. Newell, B. J. Anderson, L. Zanetti, and C. I. Meng (2005), Neutral composition effects on ionospheric storms at middle and low latitudes, *J. Geophys. Res.*, *110*, A05309, doi:10.1029/2004JA010840.
Liu, H., and S. Watanabe (2008), Seasonal variation of the longitudinal structure of the equatorial ionosphere: Does it reflect tidal influences from below?, *J. Geophys. Res.*, *113*, A08315, doi:10.1029/2008JA013027.
Liu, J., W. Wang, A. Burns, X. Yue, S. Zhang, Y. Zhang, and C. Huang (2016), Profiles of ionospheric storm-enhanced density during the 17 March 2015 great storm, *J. Geophys. Res. Space Physics*, *121*, 727–744, doi:10.1002/2015JA021832.
Maruyama, T., M. Kawamura, S. Saito, K. Nozaki, H. Kato, N. Hemmakorn, T. Boonchuk, T. Komolmis, and C. Ha Duyen (2007), Low latitude ionosphere-thermosphere dynamics studies with ionosonde chain in Southeast Asia, *Ann. Geophys.*, *25*(7), 1569–1577, doi:10.5194/angeo-25-1569-2007.
Morse, F. A., et al. (1977), Equion: An equatorial ionospheric irregularity experiment, *J. Geophys. Res.*, *82*, 578–592, doi:10.1029/JA082i004p00578.
Nygrén, T., B. S. Lanchester, A. Huuskonen, L. Jalonen, T. Turunen, H. Rishbeth, and A. P. Van Eyken (1990), Interference of tidal and gravity waves in the ionosphere and an associated sporadic *E*-layer, *J. Atmos. Sol. Terr. Phys.*, *52*, 609–613, doi:10.1016/0021-9169(90)90056-S.
Prölss, G. W. (1987), Storm-induced changes in the thermospheric composition at middle latitudes, *Planet. Space Sci.*, *35*, 807–811, doi:10.1016/0032-0633(87)90041-9.
Prölss, G. W. (1993), On explaining the local time variation of ionospheric storm effects, *Ann. Geophys.*, *11*, 1–9.
Prölss, G. W., and U. von Zahn (1974), Esro 4 Gas Analyzer results: 2. Direct measurements of changes in the neutral composition during an ionospheric storm, *J. Geophys. Res.*, *79*, 2535–2539, doi:10.1029/JA079i016p02535.
Prolss, G. W., M. Roemer, and J. W. Slowey (1988), Dissipation of solar wind energy in the Earth's upper atmosphere: The geomagnetic activity effect, CIRA, *Adv. Space Res.*, *8*(5), 215–261.
Rama Rao, P. V. S., S. Tulasi Ram, K. Niranjan, D. S. V. V. D. Prasad, S. Gopi Krishna, and N. K. M. Lakshmi (2005), VHF and L-band scintillation characteristics over an Indian low latitude station, Waltair (17.7°N, 83.3°E), *Ann. Geophys.*, *23*(7), 2457–2464, doi:10.5194/angeo-23-2457-2005.
Rama Rao, P. V. S., K. Niranjan, D. S. V. V. D. Prasad, S. Gopi Krishna, and G. Uma (2006), On the validity of the ionospheric pierce point (IPP) altitude of 350 km in the Indian equatorial and low-latitude sector, *Ann. Geophys.*, *24*, 2159–2168, doi:10.5194/angeo-24-2159-2006.
Rastogi, R. G., and R. F. Woodman (1978), VHF radio wave scattering due to range and frequency types of equatorial spread-*F*, *J. Atmos. Sol. Terr. Phys.*, *40*, 485–491, doi:10.1016/0021-9169(78)90182-4.
Rishbeth, H. (1971), Thermospheric winds and the *F*-region: A review, *J. Atmos. Terr. Phys.*, *34*, 1–47, doi:10.1016/0021-9169(72)90003-7.
Rishbeth, H. (1975), *F*-region storms and thermospheric circulation, *J. Atmos. Terr. Phys.*, *37*(6), 1055–1064, doi:10.1016/0021-9169(75)90013-6.

Rishbeth, H. (1991), F-region storms and thermospheric dynamics, *J. Geomagn. Geoelec.*, *43*(Supplement1), 513–524.
Sagawa, E., T. J. Immel, H. Frey, and S. B. Mende (2005), Longitudinal structure of the equatorial anomaly in the nighttime ionosphere observed by IMAGE/FUV, *J. Geophys. Res.*, *110*, A11302, doi:10.1029/2004JA010848.
Sastri, J. H. (1990), The relationship between the structure of the equatorial anomaly and the strength of the equatorial electrojet, *Ind. J. Radio Space Phys.*, *19*, 225–240.
Scherliess, L., and B. G. Fejer (1997), Storm time dependence of equatorial disturbance dynamo zonal electric fields, *J. Geophys. Res.*, *102*, 24,037–24,046, doi:10.1029/97JA02165.
Scherliess, L., D. C. Thompson, and R. W. Schunk (2008), Longitudinal variability of low-latitude total electron content: Tidal influences, *J. Geophys. Res.*, *113*, A01311, doi:10.1029/2007JA012480.
Seemala, G. K., and C. E. Valladares (2011), Statistics of total electron content depletions observed over the South American continent for the year 2008, *Radio Sci.*, *46*, RS5019, doi:10.1029/2011RS004722.
Shalimov, S., T. Ogawa, and Y. Otsuka (2009), On the gravity wave-driven instability of *E* layer at mid-latitude, *J. Atmos. Sol. Terr. Phys.*, *71*, 1943–1947, doi:10.1016/j.jastp.2009.08.004.
Singh, R., S. Sripathi, S. Sreekumar, S. Banola, K. Emperumal, P. Tiwari, and S. Kumar (2015), Low-latitude ionosphere response to super geomagnetic storm of 17/18 March 2015: Results from a chain of ground-based observations over Indian sector, *J. Geophys. Res. Space Physics*, *120*, 10,864–10,882, doi:10.1002/2015JA021509.
Somayajulu, V. V. (1998), Magnetosphere-Ionosphere coupling, *PINSA*, *64*(A3), 341–351.
Titheridge, J. (1985), Ionogram analysis with the generalized program POLAN, World Data Center Report, UAG-93, WDC-A-STP, Boulder,CO, 194 pp.
Titheridge, J. E. (1995), Winds in the ionosphere—A review, *J. Atmos. Sol. Terr. Phys.*, *57*(14), 1681–1714, doi:10.1016/0021-9169(95)00091-F.
Tsurutani, B. T., and W. D. Gonzalez (1997), The interplanetary causes of magnetic storms: A review, in *Magnetic Storms*, edited by B. T. Tsurutani et al., 77 pp., AGU, Washington, D. C., doi:10.1029/GM098p0077.
Tsurutani, B. T., W. D. Gonzalez, and Y. Kamide (1997), Magnetic storms, *Surv. Geophys.*, *18*, 363–383, doi:10.1023/A:1006555215463.
Tulasi Ram, S., et al. (2016), Duskside enhancement of equatorial zonal electric field response to convection electric fields during the St. Patrick's Day storm on 17 March 2015, *J. Geophys. Res. Space Physics*, *121*, 538–548, doi:10.1002/2015JA021932.
Wei, Y., W. Wan, Z. Pu, M. Hong, Q. Zong, J. Guo, B. Zhao, and Z. Ren (2011), The transition to overshielding after sharp and gradual interplanetary magnetic field northward turning, *J. Geophys. Res.*, *116*, A01211, doi:10.1029/2010JA015985.
Wolf, R. A. (1975), Ionosphere-magnetosphere coupling, *Space Sci. Rev.*, *17*, 537–562, doi:10.1007/BF00718584.